ISSN 2411-3336; e-ISSN 2541-9404

JOURNAL OF MINING INSTITUTE

Zapiski Gornogo instituta

Journal homepage: pmi.spmi.ru

*Research article* *Geology*

# Lithological characteristics of lacustrine sediments in lakes Bolshoye Miassovo and Maloye Miassovo (Southern Urals, Russia)

**Anastasiya R. Yusupova✉, Nouria G. Nourgalieva**
*Kazan Federal University, Kazan, Republic of Tatarstan, Russia*

***How to cite this article:*** Yusupova A.R., Nourgalieva N.G. Lithological characteristics of lacustrine sediments in lakes Bolshoye Miassovo and Maloye Miassovo (Southern Urals, Russia). Journal of Mining Institute. 2026. Vol. 280, p. 47-69.

***Abstract***
Climate is one of the key factors controlling sediment accumulation in lacustrine ecosystems. Integrated studies of continuous lake-sediment cores, including radiocarbon dating, grain-size analysis, mineralogical and chemical characterization, and measurements of magnetic properties, enable reconstructions of sedimentation conditions during the Late Quaternary. Such studies are particularly relevant for lakes of the Southern Urals, which are located near a climatic divide and for which episodes of increasing/decreasing moisture have been interpreted inconsistently. This paper presents data on the age, material composition, and genetic features of bottom sediments from lakes Bolshoye Miassovo and Maloye Miassovo. The results show that, based on grain-size distribution, mineral composition, and inorganic geochemistry, the studied lacustrine sediments exhibit a pattern typical of freshwater lakes – the predominance of allothigenic silt-sized particles. This is supported by the structure of allothigenic-input factor F1 derived from factor analysis. Quaternary deposits represented by eluvial, slopewash, colluvial, and alluvial facies were identified as the main source of allothigenic material for the investigated basins. The ICV index and the A-CN-K diagram indicate that the sediments formed predominantly from stable allothigenic minerals of the primary sedimentation cycle, sourced mainly from Quaternary deposits and exposed pre-Quaternary rocks. The transport pathways of allothigenic material are linked to the directions of slope flows and channel networks visible on the Quaternary-deposit map. The integrated analysis allowed us to identify the most informative proxies and to correlate them with global and regional climatic stages and events, including the Bølling warming (~14,700 cal. yr BP), the ~8200 cal. yr BP cooling event, aridization in the Southern Urals (~2000 cal. yr BP), and Bond Event 1 (~1500 cal. yr BP). Additional climate-arid events were identified at ~11,430, ~6100, ~4250, ~3537, and ~1065 cal. yr BP.

***Keywords***
modern lake sediments; radiocarbon dating; grain-size analysis; geochemistry; mineral composition; factor analysis; paleoclimate; Holocene; Late Pleistocene

***Funding***
This work was funded by the subsidy allocated to Kazan Federal University for the State assignment in the sphere of scientific activities (project N FZSM-2023-0023).

***Received: 14.08.2025*** ***Accepted: 24.12.2025*** ***Online: 01.07.2026*** ***Published: 10.09.2026***

## Introduction

At present, because of the high probability of climate-related hazards and the need to adapt to ongoing climate change, understanding modern environmental and climatic change has become a pressing issue. Studying the causes of climate change in past epochs is an important part of climate-evolution research and is of fundamental interest [1-3]. Bottom sediments of modern lakes are geochemical and mineralogical archives. Their study is useful for understanding regional and global climate change [1]. At the same time, the geochemistry of lake sediments can reflect the complexity of processes occurring not only within the lake itself but also within its catchment [4]. Climate affects the distribution of chemical elements in modern lake sediments because temperature and moisture largely govern the intensity of near-surface weathering, soil formation, and sedimentation through interactions among the atmosphere, hydrosphere, biosphere, and lithosphere [5]. Different ratios of mobile and immobile elements therefore record changes in the direction and intensity of these processes [5]. The chemical composition of lake sediments, in turn, determines their mineral composition. The mineral assemblage reflects the relative contributions of detrital, chemogenic, and biogenic material, which vary with climate. Climate controls allothigenic input, lake-level fluctuations, and lake productivity [6]. Allothigenic material is typically represented by mature minerals and is related to the composition of the source province and (or) the catchment area. Authigenic minerals are usually represented by carbonates, sulfates, chlorides, and sulfides [6].

The Southern Urals, owing to their geographic position, complex geological structure, and climate sensitivity, have attracted increasing research interest [6-8]. Among the representative lakes of the Southern Urals with thick sediment sequences are lakes Bolshoye Miassovo and Maloye Miassovo [7-9]. To date, these lakes have been studied in several respects.

The increase in lake-water mineralization in the Southern Urals over the last 100 years has been linked to climate warming in this area. For sediment cores from lakes Bolshoye Miassovo and Maloye Miassovo spanning the Late Pleistocene – Holocene, preliminary data on chemical and mineral composition have been reported [9]. A diatom analysis of sediments from Bolshoye Miassovo Lake [8] characterized the main stages of lake evolution during the Late Quaternary. A spore-pollen analysis [7] reconstructed vegetation cover within the lake catchment and the regional climatic conditions over the last 13,400 cal. yr BP.

The aim of this study is to identify the structure and material-composition features formed under climatic change during the Late Pleistocene and Holocene using long sediment cores from lakes Bolshoye Miassovo and Maloye Miassovo. For the first time in the Southern Urals, we compare sedimentary sequences from two nearby lakes using an integrated set of material proxies-grain-size, mineralogical and geochemical analyses, and magnetic parameters. This approach advances our understanding of Late Quaternary climate change.

**Geographical setting and geological characteristics of the study area**

Lakes Bolshoye Miassovo (55°09'59.89" N; 60°20'51.82" E) and Maloye Miassovo (55°10'04" N; 60°21'08" E) are located in the Southern Urals. They are situated within the Ural mountain-ridge zone and within the contact zone between an erosional-abrasional platform (the Trans-Ural peneplain) and the West Siberian Lowland [10].

According to the geological map of pre-Quaternary bedrock, the western margin of the studied lake group is composed mainly of rocks of the Yelanchikov formation ($PR_1el$), represented by plagiogneisses and migmatites (Fig.1, *a*). The plagiogneisses include biotite, amphibole-biotite, garnet-biotite, and sillimanite-garnet-biotite varieties. Migmatites are characterized by the predominance of plagioclase over K-feldspar. Compared with rocks of the Ilmenogorsk formation, both felsic and mafic rocks of the Yelanchikov formation show somewhat higher $Al_2O_3$ contents, lower Fe contents, and higher Ca contents. The southern and southeastern margin of the lake group is composed of rocks of the Uvildy-Kisegach monzodiorite-granosyenite-granite complex, the Kagan complex of metamorphosed ultramafic rocks and gabbroids, and rocks of the Kyshtym formation. The northern margin is composed of pre-Quaternary rocks of the following complexes and suites: the Yelanchikov formation, the Baik complex of metamorphosed ultramafics and gabbroids, the Verkhnesait and Igish suites, and the Urazbaev complex. These rocks are represented by biotite gneisses, enstatite-olivine rocks, graphite-bearing quartzites, garnet and pyroxene amphibolites, biotite plagiogneisses, staurolite-garnet-biotite rocks, micaceous quartzites, and marble.

**Journal of Mining Institute.** 2026. Vol. 280. P. 47-69


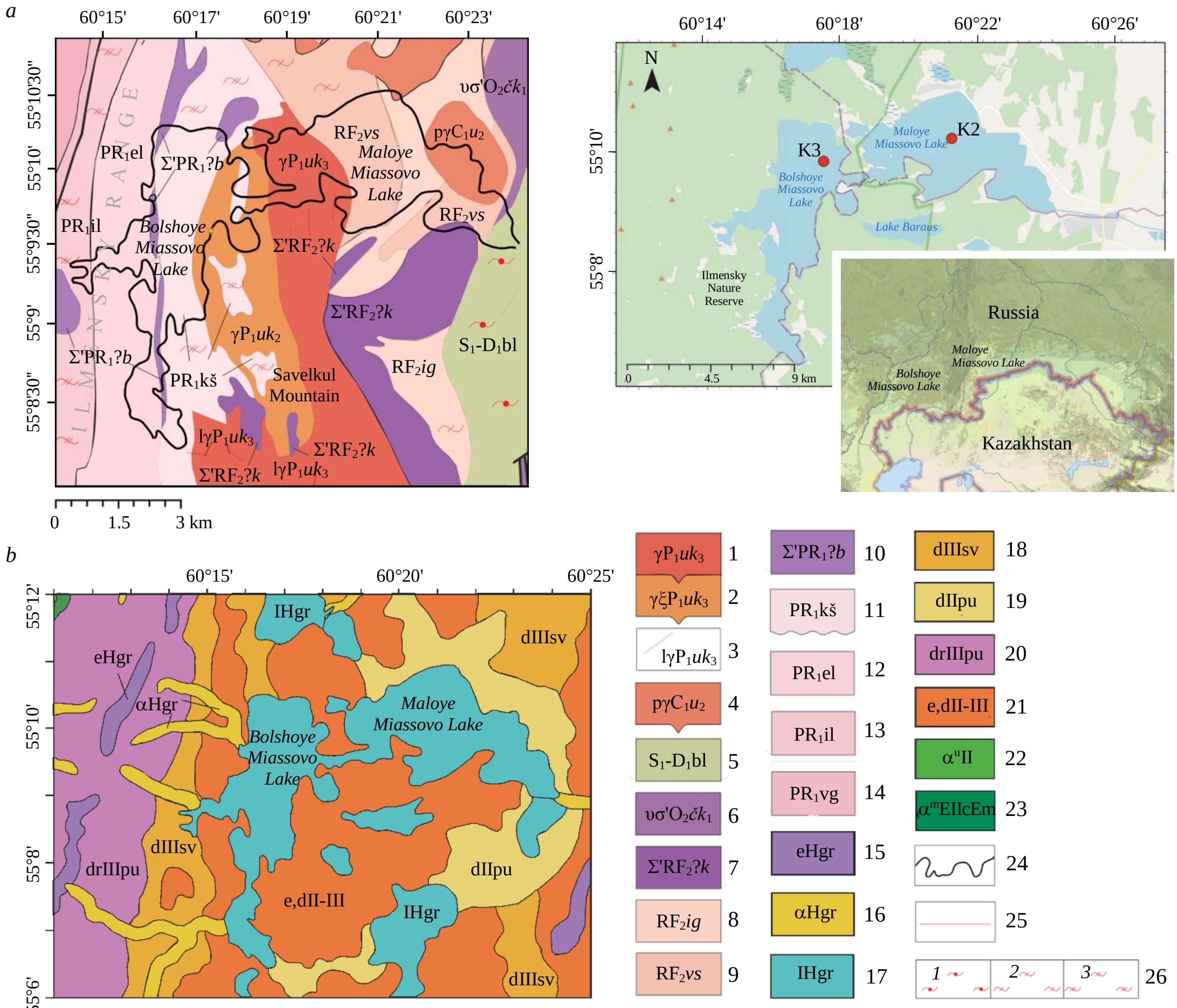


Fig.1. Schematic geological maps of the area of lakes Bolshoye Miassovo and Maloye Miassovo: *a* – pre-Quaternary bedrock; *b* – Quaternary deposits (based on the State geological map of the Russian Federation, scale 1:200,000, sheet N-41-VII)

1 – Uvildy-Kisegach monzodiorite-granosyenite-granite complex; 2, 3 – phases (2 – second phase: granosyenites, porphyritic granites, 3 – third phase: biotite granites, leucogranites, leucogranite, pegmatite dikes); 4 – Urazbaev tonalite-plagiogranite complex (plagiogranites); 5 – Bulatov formation (carbonaceous-siliceous schists, quartzites, metabasalt, and metatuff ($\geq$ 900 m); 6 – Chebarkul-Kazbaev complex of serpentinized rocks (after dunites, harzburgites, and gabbro); first phase (serpentinites after dunites and harzburgites, less commonly after pyroxenites, antigorite serpentinites, talc-carbonate rocks); 7 – Kagan complex of metamorphosed ultramafic and gabbroic rocks (antigorite serpentinites, olivine-antigorite, olivine-talc, enstatite-talc-anthophyllite, and tremolite rocks, rarely clinopyroxenites and gabbroic rocks, talcites); 8, 9 – suites: 8 – Igish Suite (graphite-bearing quartzites, phosphate-bearing quartzites, interbeds of garnet-biotite and staurolite-garnet-biotite plagioclase schists (400-500 m), 9 – Verkhnesait Suite (amphibole plagioclase schists, garnet-biotite-amphibole schists, amphibole-biotite, biotite, and garnet-biotite schists, interbeds of graphite-bearing and phosphate-bearing quartzites (560 m); 10-14 – Ilmenogorsky Uplift: 10 – Baik complex of metamorphosed ultramafic and gabbroic rocks: enstatite-olivine rocks and related serpentinites, olivine-amphibole-enstatite rocks, anthophyllite rocks, tremolite rocks, tremolite-talc-anthophyllite rocks, talc-carbonate rocks, metagabbro; 11-14 – formations: 11 – Kyshtym formation: amphibolites, including garnet-bearing, biotite, garnet-biotite, and two-mica gneisses, mica-quartz schists, quartzites, interbeds of marble (900 m), 12 – Yelanchikov formation: biotite gneisses, less commonly garnet-biotite and amphibole-biotite gneisses, amphibolites; interbeds of graphite-bearing quartzites (1300 m), 13 – Ilmenogorsk formation: amphibolites, including biotite-, garnet-, and pyroxene-bearing, biotite and amphibole-biotite plagiogneisses, garnet-biotite plagiogneisses with sillimanite, garnet-biotite and graphite-bearing quartzites, pyroxene-plagioclase crystalline schists (600-1110 m), 14 – Vishnevogorsk formation: biotite plagiogneisses, garnet-biotite plagiogneisses with graphite and sillimanite, amphibolites, including garnet- and pyroxene-bearing, diopside-plagioclase crystalline schists, calc-silicate rocks, marbles (500-1800 m); 15-17 – Holocene: 15 – eluvial deposits: blocky-gravelly bedrock debris (up to 1.5 m), GU zone, 16 – alluvial deposits of floodplain terraces and channels: polymictic sands with gravel, silty and peaty clays, pebbles and boulders (up to 10 m), 17 – lacustrine deposits: sands, silt, and silty clays (up to 2 m); 18-23 – Pleistocene: 18-21 – Neopleistocene, Middle-Upper units (18 – Severouralsky superhorizon: slopewash deposits, brown loams with grus, crushed stone, and rare gravel of local rocks (up to 6 m), 19 – Polyarnouralsky horizon: slopewash deposits, clays with rare crushed stone of underlying rocks and rare gravel (up to 5 m), MU zone, 20 – Polyarnouralsky horizon: colluvial deposits, blocks, crushed stone, sandy clays with crushed stone (up to 5 m), GU zone, 21 – eluvial and slopewash deposits: weathered crushed stone of underlying rocks with a loamy matrix; grus and rare pebbles (up to 2 m); 22, 23 – Eopleistocene, Upper unit: 22 – alluvial deposits of the Ufa terrace: loams, polymictic sands, interbeds of gravel with pebbles (up to 20 m), GU zone, 23 – Chumlyak horizon: alluvial deposits of the Miass terrace, polymictic sands with an admixture of gravel, loams with buried soils, gravel and pebbles (up to 20 m), GU zone; 24 – shorelines of lakes Bolshoye Miassovo and Maloye Miassovo; 25 – faults; 26 – metamorphic facies: *1* – greenschist, *2* – epidote-amphibolite, *3* – amphibolite. K2, K3 – sediment-core sampling sites

The Quaternary-deposit map shows that the shores of lakes Bolshoye Miassovo and Maloye Miassovo are bordered by eluvial and slopewash deposits (e,dII-III). These deposits are represented by gravel and grus of weathered rocks with rare quartz pebbles, cemented by brown clays [11] (Fig.1, *b*). On the western and northern shores of Bolshoye Miassovo Lake, slopewash deposits of the Severouralsky superhorizon (Neopleistocene) are present (Fig.1, *b*). On the western shore of Bolshoye Miassovo Lake, Holocene alluvial deposits of floodplain terraces and channels are also present; they consist of polymictic sands with gravel, silty clays, pebbles, and boulders (Fig.1, *b*). The northern, eastern, and southeastern shores of Maloye Miassovo Lake are composed of slopewash deposits of the Polyarnouralsky horizon (Neopleistocene), represented by clays with rare gravel of the underlying rocks and rare gravel-sized material [11] (Fig.1, *b*). The thickness of Quaternary deposits rarely exceeds 10 m. Smaller thicknesses are observed in the west compared with the rest of the framing of the studied lakes.

**Materials and methods**

Material was collected during a scientific expedition in 2018. Detailed investigations were carried out for sediment core N 3 (55°09'51.1" N; 60°17'21.9" E) from Bolshoye Miassovo Lake (depth of 24 m) and sediment core N 2 (55°10'13.6" N; 60°21'04.6" E) from Maloye Miassovo Lake (depth of 7 m) (points К3, К2, Fig.1, *a*). The cores were selected based on preliminary seismoacoustic surveys and rapid measurements of magnetic susceptibility. Samples were taken at 2-centimeter intervals.

Based on the primary lithological description conducted in the field, the sediment sequence of Bolshoye Miassovo Lake consists of dark-green, dense mud with abundant plant remains (interval 526-2 cm, thickness 526 cm). The upper part of the Maloye Miassovo Lake core (interval 422-2 cm, thickness 422 cm) is also composed of dark-green, dense mud with abundant plant remains. The lower part of this core (interval 512-422 cm, thickness 92 cm) consists of dense gray clayey mud. The samples were packed in plastic bags and delivered to the Laboratory of paleoclimatology, paleoecology, and paleomagnetism of Institute of Geology and Petroleum Technologies of Kazan Federal University, for subsequent comprehensive laboratory analyses.

Preliminary magnetic-property data and the primary lithological description were used to select samples for radiocarbon dating (nine samples from each site). Prepared samples were sent to NTUAMS Lab of National Taiwan University. Measurements were performed using a 1.0 MV HVE accelerator mass spectrometer. Sample ages were calibrated using OxCal 4.2.4 [12] and the IntCal20 calibration curve. Detailed procedures for sample preparation and measurements are described in [13]. Radiocarbon-dating results and the age model for Bolshoye Miassovo Lake sediments are presented in [7].

Lithological types of the studied deposits were determined by laser grain-size analysis. Initial sample pretreatment included digestion with 10 % HCl and 30 % $H_2O_2$ to remove carbonate and organic matter. Measurements were performed with an LS 13 320 XR particle-size analyzer (Beckman Coulter, USA) equipped with a universal liquid module. The analyzer was calibrated and internal quality control was performed using reference materials. Blanks (distilled water) were measured to control the background signal. Background was checked before each measurement; if an unacceptable background level (> 10 %) was obtained, the cuvette was washed. A background signal < 10 % was accounted for by the software when calculating the particle-size distribution. The resulting histograms show the distribution of size fractions. We also calculated the median grain size (Md), which reflects the energy of the hydrodynamic environment and lacustrine accommodation. Lithological types were classified using the classification of unlithified sediments proposed by N.V.Logvinenko.

Changes in the ratio of allothigenic and authigenic minerals are known to be informative for reconstructing depositional conditions, including climatic conditions [6, 9]. Mineral composition was determined using a D2 PHASER X-ray diffractometer. The measurement settings were as follows:

X-ray tube voltage 30 kV; current 10 mA; step size 0.02°; scan speed 1°/min; Bragg – Brentano geometry; 2θ range 3-40°. Data were interpreted using DIFFRACplus Evaluation Package – EVA, Search/Match (Bruker, Germany) to perform qualitative and quantitative analyses. Analytical accuracy was ±0.02° across the entire range. The obtained diffractograms were compared with reference patterns in a computerized database. Principal d-spacings were determined and assigned to specific mineral phases. The PDF-2 international powder diffraction database was used. Quantitative analysis was performed in Topas program (Bruker, Germany) using full-profile Rietveld refinement. To investigate the morphology and elemental composition of mineral particles in the bottom sediments of the studied lakes, and to identify allothigenic/authigenic minerals, samples were examined by scanning electron microscopy. Analyses were carried out using a Merlin field-emission scanning electron microscope (Carl Zeiss, Germany) at the Interdisciplinary Center "Analytical Microscopy" of Kazan Federal University. The instrument is equipped with an Aztec X-MAX energy dispersive spectroscopy detector, energy resolution is 127 eV. Measurement accuracy is 0.01-1 %, depending on the state of the analyzed object. Surface morphology was imaged at an accelerating voltage of 5 keV to increase depth of field. Elemental analysis was performed at 20 keV and a working distance of 9 mm, which minimized analytical errors. The interaction depth was less than 1 μm.

Major and trace element contents were determined using a Bruker S8 Tiger X-ray fluorescence (XRF) spectrometer. Sample preparation included grinding the material to a particle size of 40-50 μm and pressing it with boric acid in a 20-ton press to produce a pellet with a flat surface. The pellet was then placed in the instrument for analysis. Instrument calibration was performed using standard reference materials. The matrix in the standards was $SiO_2$, which allows matrix effects to be taken into account when analyzing all other elements. Loss on ignition (LOI) was determined as follows. Aliquots of the studied samples (~ 0.5 g) were placed into ceramic crucibles and covered with 10 % HCl for 24 h. This treatment removed carbon contained in the sediment. The crucibles were then ignited in an SNOL1100 muffle furnace at 900 °C for 4 h. After cooling, the residue was weighed and LOI values were calculated.

Statistical processing was performed using Statistica software package. For the entire geochemical dataset from lakes Bolshoye Miassovo and Maloye Miassovo, correlation analysis was carried out using Spearman's nonparametric coefficient $R$ at a significance level of $p < 0.05$. To better resolve the genetic characteristics of the studied objects, the geochemical datasets were tested for normality. Factor analysis was then performed using principal component analysis with "Varimax normalized" rotation. We also calculated the index of compositional variability as $ICV = [(Fe_2O_3 + K_2O + Na_2O + CaO + MgO + MnO + TiO_2) / Al_2O_3]$. Values of ICV < 1 indicate weathering/maturity, and values of ICV > 1 indicate the opposite [14].

For all samples from the studied sediment cores from lakes Maloye Miassovo and Bolshoye Miassovo, normal remanent magnetization curves were obtained during a continuous increase in the external magnetic field up to 1.5 T. Measurements were performed using a J_meter coercivity spectrometer [15]. The magnetic moment sensitivity of the $J_r$ channel (remanent magnetization) is $\sim 1 \cdot 10^{-8}$ A·m$^2$, and that of the $J_i$ (induced magnetization) is $\sim 1 \cdot 10^{-6}$ A·m$^2$. The maximum induction of the magnetizing field is 1500 mT. Sample preparation for magnetic measurements included drying, grinding in a non-magnetic agate mortar, and packing into specialized paper containers. Each sample was weighed before measurement because sample mass is accounted for during the measurements. As a result, complete hysteresis loops were obtained simultaneously for remanent and induced magnetization. Based on the normal magnetization curves, the contributions of different components to the magnetic signal of the sediment were determined – ferromagnetic (k_ferro), dia-/paramagnetic (k_para), and superparamagnetic (k_super), following the procedure described in [16]. In general, the paramagnetic component reflects the influx of allothigenic material into the depositional basin.

**Journal of Mining Institute.** 2026. Vol. 280. P. 47-69


Ferromagnetic material has a mixed origin (allothigenic and biogenic). Superparamagnetic minerals may also be of either biogenic or allothigenic origin; superparamagnetic grains may be represented by hematite or by biogenically induced iron oxides or sulfides [16]. To perform correlation analysis between magnetic parameters and the factor-analysis results, the resulting dataset was tested for normality.

## Results

*Radiocarbon dating*. In study [7] it was established that sedimentation in Bolshoye Miassovo Lake began no later than ~13,400 cal. yr BP. Table 1 presents the results of radiocarbon dating of sediments from Maloye Miassovo Lake; according to these data, sedimentation in the lake began no later than ~20,100 cal. yr BP. The mean sediment-accumulation rate was ~0.32 mm/year (Fig.2, *a*).

*Table 1*

**Radiocarbon dating results for bottom sediments from Maloye Miassovo Lake***

| Laboratory ID | Sample number | Depth, cm | Dated material | AMS $^{14}C$ age, $^{14}C$ yr BP | Calibrated $^{14}C$ age, cal. yr BP |
|---|---|---|---|---|---|
| NTUAMS-5023-1 | 116 | 30 | Lake sediment | 123±78 | 80±80 |
| NTUAMS-5024-1 | 147 | 92 | | 1987±82 | 1920±205 |
| NTUAMS-5025-1 | 193 | 184 | | 3396±82 | 3650±200 |
| NTUAMS-5026-1 | 236 | 270 | | 4823±87 | 5585±150 |
| NTUAMS-5027-1 | 265 | 328 | | 6814±87 | 7700±140 |
| NTUAMS-8498-1 | 287 | 374 | | 8216±83 | 9175±165 |
| NTUAMS-50281 | 306 | 410 | | 9496±85 | 10,840±275 |
| NTUAMS-5029-1 | 323 | 444 | | 11,443±95 | 13,330±165 |
| NTUAMS-5031 | 355 | 508 | | 16,462±233 | 19,915±545 |

* Radiocarbon ages are reported in years before present with the associated statistical uncertainty; “present” is defined as AD 1950.

*Grain-size composition.* According to the data obtained, the silt fraction predominates in sediments of both lakes (Table 2, Fig.2, *b*). Sand and clay fractions are less abundant (Table 2, Fig.2, *b*). The sediment core from Bolshoye Miassovo Lake consists mainly of interbedded light silty loam and silty sandy loam (Fig.2, *b*). The lower part of the core is represented by sandy loam (Fig.2, *b*).

*Table 2*

**Grain-size composition of sediments from lakes Bolshoye Miassovo and Maloye Miassovo, %**

| Lake | Silt | Sand | Clay | Md, mm |
|---|---|---|---|---|
| Bolshoye Miassovo | 43.33-79.07<br>67.48 | 10.00-49.10<br>21.73 | 7.29-16.93<br>10.79 | 0.01-0.05<br>0.02 |
| Maloye Miassovo | 47.23-74.12<br>64.92 | 13.22-40.67<br>23.70 | 5.58-19.60<br>11.37 | 0.02-0.04<br>0.02 |

*Note.* The numerator shows the minimum and maximum values, and the denominator shows the mean value.

In the Late Pleistocene (interval 522-502 cm, ~13,400-13,220 cal. yr BP), the sediment is represented by sandy loam, and Md is ~ 0.046 mm. Upsection (interval 502-346 cm, ~13,220-7500 cal. yr BP), Md values decrease sharply (Fig.2, *b*), with a mean of ~0.021 mm. This interval is characterized by alternation of silty sandy loam and light silty loam. A distinct event is recorded at a depth of 322 cm (~6760 cal. yr BP), where Md increases to ~0.033 mm, corresponding to the Holocene thermal maximum. The interval 322-142 cm (~6760-2600 cal. yr BP) is characterized by alternation of light silty loam and silty sandy loam; mean Md is ~0.024 mm. In the interval 142-8 cm (Subatlantic stage, ~2600-790 cal. yr BP), silt fraction predominates (Fig.2, *b*), and light silty loam is dominant. Md values are minimal, mean value is ~ 0.017 mm.

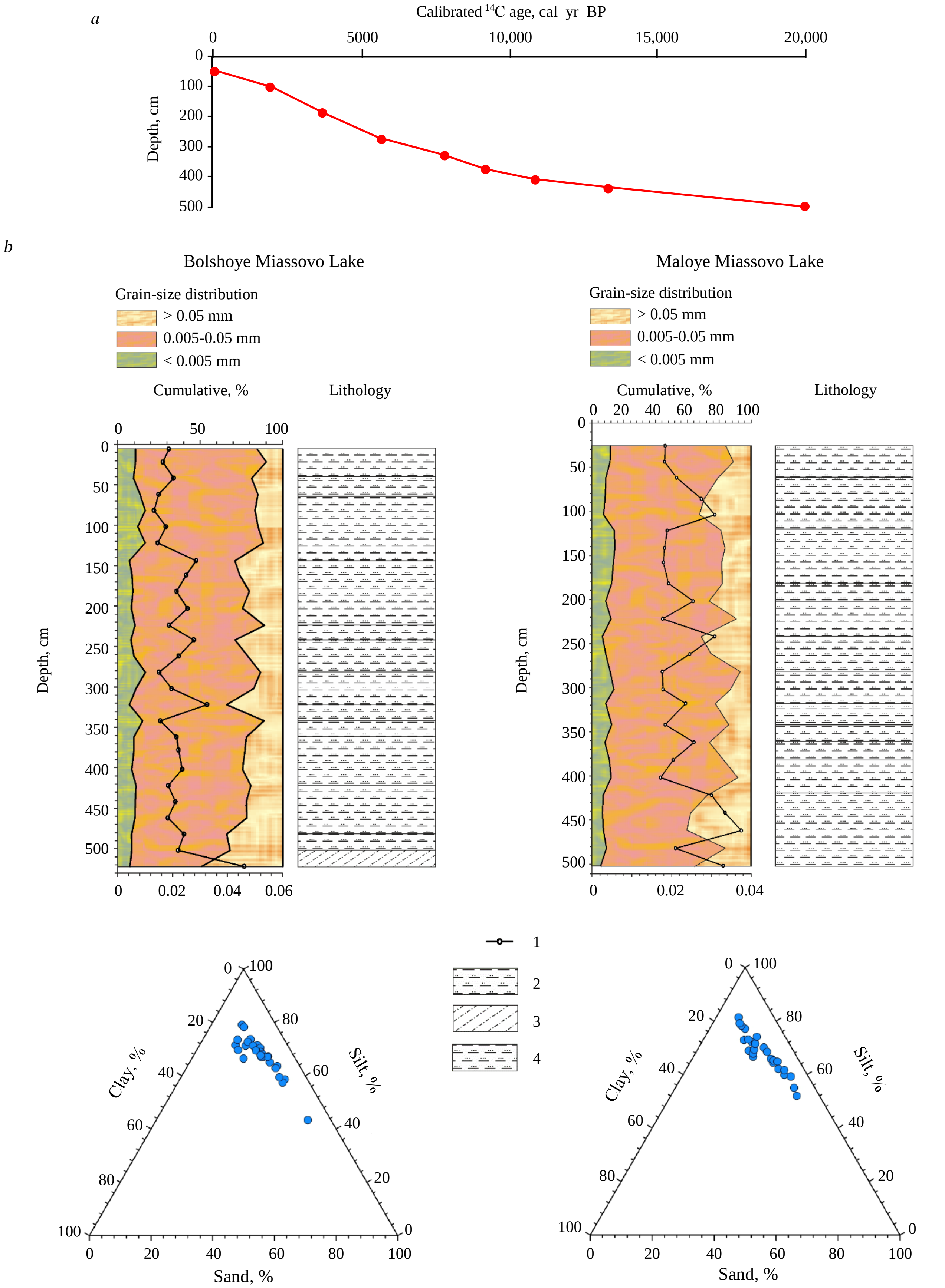


Fig.2. Age-depth model for sediments of Maloye Miassovo Lake (*a*); results of grain-size analysis for lakes Bolshoye Miassovo and Maloye Miassovo (*b*)

1 – Md, mm; 2 – light silty loam; 3 – sandy loam; 4 – silty sandy loam

The sediment sequence of Maloye Miassovo Lake is characterized by interbedding of light silty loam and silty sandy loam (Fig.2, *b*). The Pleistocene part of the Maloye Miassovo Lake core (interval 502-422 cm) is characterized by a substantial presence of the psammitic (sand) fraction (up to 40.67 %). Lithologically, the Late Pleistocene sediments are represented by silty sandy loam. The mean Md during this period is 0.03 mm. The interval 422-402 cm (beginning of the Holocene, Preboreal stage to the beginning of the Boreal stage) is characterized by a noticeable increase in the silt fraction and a marked decrease in Md to 0.015 mm. The sediments are represented by light silty loam. In the interval 402-382 cm (end of the Boreal stage), the content of the psammitic fraction increases, and Md also increases to 0.026 mm. The sediment is represented by silty sandy loam. In the interval 382-282 cm (Atlantic stage), interbedding of light silty loam and silty sandy loam is typical. Md varies within 0.018-0.024 mm. The highest Md value corresponds to the middle of the Atlantic stage (depth 318 cm, ~7200 cal. yr BP), which coincides with the Holocene thermal maximum. Sediments of the Subboreal stage are represented by interbedding of light silty loam and silty sandy loam. In the interval 262-142 cm (Subboreal stage), a pronounced increase in Md to 0.031 mm is observed (depth 242 cm, ~4900 cal. yr BP). A small increase in Md during the Subboreal stage is also recorded at 202 cm (~4000 cal. yr BP). For the Subatlantic stage (122-26 cm), an increase in Md to 0.031 mm is observed at 104 cm (~2100 cal. yr BP).

*Mineral composition*. X-ray diffraction analysis showed that sediments from the studied lakes are characterized by the predominance of allothigenic minerals (Table 3).

*Table 3*

**Mineral composition of sediments from lakes Bolshoye Miassovo and Maloye Miassovo, %**

| Lake | Allothigenic minerals | Opal + + cristobalite + + tridymite | Pyrite | Gypsum | Calcite |
|---|---|---|---|---|---|
| Bolshoye Miassovo | 49-80<br>63 | 6-36<br>24 | 1-9<br>4 | 2-26<br>7 | 2-19<br>9 |
| Maloye Miassovo | 20-84<br>71 | 9-26<br>15 | 1-5<br>2 | 2-77<br>14 | 3-20<br>7 |

*Note*. The numerator shows the minimum and maximum values, and the denominator shows the mean value.

In sediments of Bolshoye Miassovo Lake, allothigenic minerals are represented by quartz, microcline, albite, mica, chlorite, and amphiboles. In sediments of Maloye Miassovo Lake, in addition to the minerals listed above, talc and mixed-layer clay minerals were identified (Fig. 3, *a*). Biogenic silica was recorded in sediments from both lakes (Fig.4, image 3, Fig.5, images 1, 6). Its abundance was assessed from the content of opal + cristobalite + tridymite (see Fig.3, *a*), which are associated with an X-ray amorphous biogenic component. This component includes material derived from diverse diatom frustules and stomatocysts (see Fig.4, image 3) [17]. Scanning electron microscopy showed that stomatocysts are spherical and mostly have smooth surfaces, with sizes of 5-10 μm (see Fig.4, image 3, Fig.5, images 1, 6) [18]. Authigenic pyrite was identified using scanning electron microscopy (see Fig.4, image 10, Fig.5, images 3, 11). Carbonate minerals were also detected in sediments from the studied lakes, including calcite (see Fig.3, *b*, Fig.4, images 1, 11, Fig.5, image 9), aragonite (see Fig.4, images 4, 6, 7, 9, Fig.5, image 4) and dolomite (see Fig.4, image 5, Fig.5, images 8, 10). Sulfates in sediments of lakes Maloye Miassovo and Bolshoye Miassovo are represented by gypsum (see Fig.3, Fig.4, image 8, Fig.5, images 2, 5, 7) and barite (see Fig.4, image 2). Iron oxides were also recorded in sediments of Bolshoye Miassovo Lake (see Fig.4, image 12).

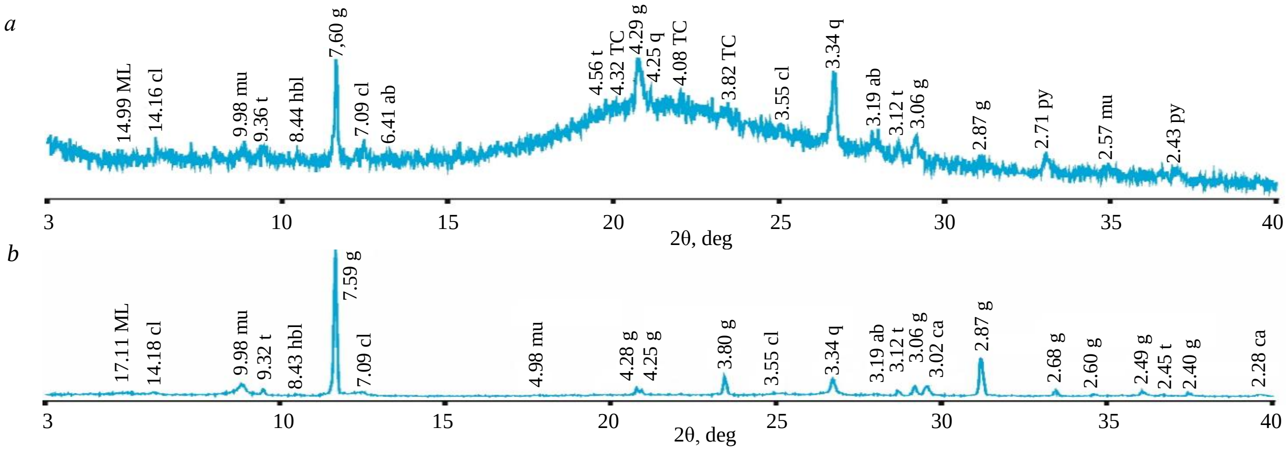


Fig.3. X-ray diffraction patterns from depths 20 cm (*a*) and 500 cm (*b*)
ML – mixed-layer clay minerals; TC – tridymite-cristobalite phase; cl – chlorite; mu – muscovite; t – talc; hbl – hornblende; g – gypsum; ab – albite; q – quartz; py – pyrite; ca – calcite

*Chemical composition of sediments based on XRF data*. Table 4 presents data on the contents of major chemical elements in sediments from lakes Bolshoye Miassovo and Maloye Miassovo. Among trace components in the sediments, the presence of Cl, BaO, SrO, Br, $V_2O_5$, ZnO, NiO, $Cr_2O_3$, CuO, $MoO_3$, $ZrO_2$, $Rb_2O$, CoO was identified, with mean contents, wt.%: 0.05; 0.0238; 0.019; 0.0135; 0.0126; 0.0095; 0.0078; 0.0075; 0.0058; 0.0041; 0.0040; 0.0033; 0.0012. In addition, along the sediment core from Bolshoye Miassovo Lake, $UO_2$ was detected in six samples (mean content 0.0056 wt.%), $Nb_2O_5$ was detected in two samples (mean content 0.0012 wt.%) and $Y_2O_3$ was detected in one sample (mean content 0.0012 wt.%). In sediments from Maloye Miassovo Lake, the presence of Cl, BaO, SrO, Br, NiO, $Cr_2O_3$, $V_2O_5$, ZnO, was recorded, with mean contents, wt.%: 0.051; 0.025; 0.018; 0.010; 0.015; 0.015; 0.013; 0.01. Less common trace components in sediments of Maloye Miassovo Lake include CuO, PbO, $ZrO_2$, $Y_2O_3$, $Rb_2O$, $Ga_2O_3$, $As_2O_3$, CoO, with mean contents, wt.%: 0.007; 0.005; 0.005; 0.004; 0.003; 0.002; 0.002; 0.0015.

*Table 4*

**Descriptive statistics for major-element contents in sediments of lakes Bolshoye Miassovo and Maloye Miassovo, wt.%**

| Component | Minimum | Maximum | Mean | Standard deviation | Number of samples |
|---|---|---|---|---|---|
| Bolshoye Miassovo Lake | | | | | |
| $SiO_2$ | 19.0 | 40.1 | 30.6 | 5.1 | 53 |
| $TiO_2$ | 0.1 | 0.7 | 0.2 | 0.1 | 53 |
| $Al_2O_3$ | 1.6 | 9.9 | 3.6 | 2.1 | 53 |
| $Fe_2O_3$ | 2.0 | 7.3 | 3.6 | 1.1 | 53 |
| MnO | 0.1 | 0.6 | 0.2 | 0.1 | 53 |
| MgO | 0.5 | 4.3 | 1.3 | 0.9 | 53 |
| CaO | 0.7 | 20.5 | 4.4 | 6.0 | 53 |
| $Na_2O$ | 0.0 | 0.7 | 0.3 | 0.2 | 53 |
| $K_2O$ | 0.3 | 2.3 | 0.7 | 0.5 | 53 |
| $P_2O_5$ | 0.3 | 0.7 | 0.5 | 0.1 | 53 |
| $SO_3$ | 3.01 | 18.7 | 6.2 | 3.5 | 53 |
| LOI | 22.6 | 58.6 | 48.2 | 10.2 | 53 |
| Maloye Miassovo Lake | | | | | |
| $SiO_2$ | 8.0 | 47.9 | 18.5 | 6.5 | 52 |
| $TiO_2$ | 0.1 | 0.9 | 0.3 | 0.1 | 52 |
| $Al_2O_3$ | 2.1 | 17.6 | 5.2 | 2.7 | 52 |
| $Fe_2O_3$ | 1.0 | 8.1 | 3.5 | 1.4 | 52 |
| MnO | 0.0 | 0.5 | 0.1 | 0.1 | 52 |
| MgO | 1.0 | 4.5 | 2.1 | 0.8 | 52 |
| CaO | 1.2 | 29.5 | 5.5 | 7.8 | 52 |
| $Na_2O$ | 0.2 | 0.7 | 0.3 | 0.1 | 49 |
| $K_2O$ | 0.3 | 2.6 | 0.8 | 0.5 | 52 |
| $P_2O_5$ | 0.3 | 0.8 | 0.4 | 0.1 | 52 |
| $SO_3$ | 1.1 | 30.7 | 7.2 | 6.2 | 52 |
| LOI | 22.5 | 75.9 | 56.8 | 15.6 | 52 |

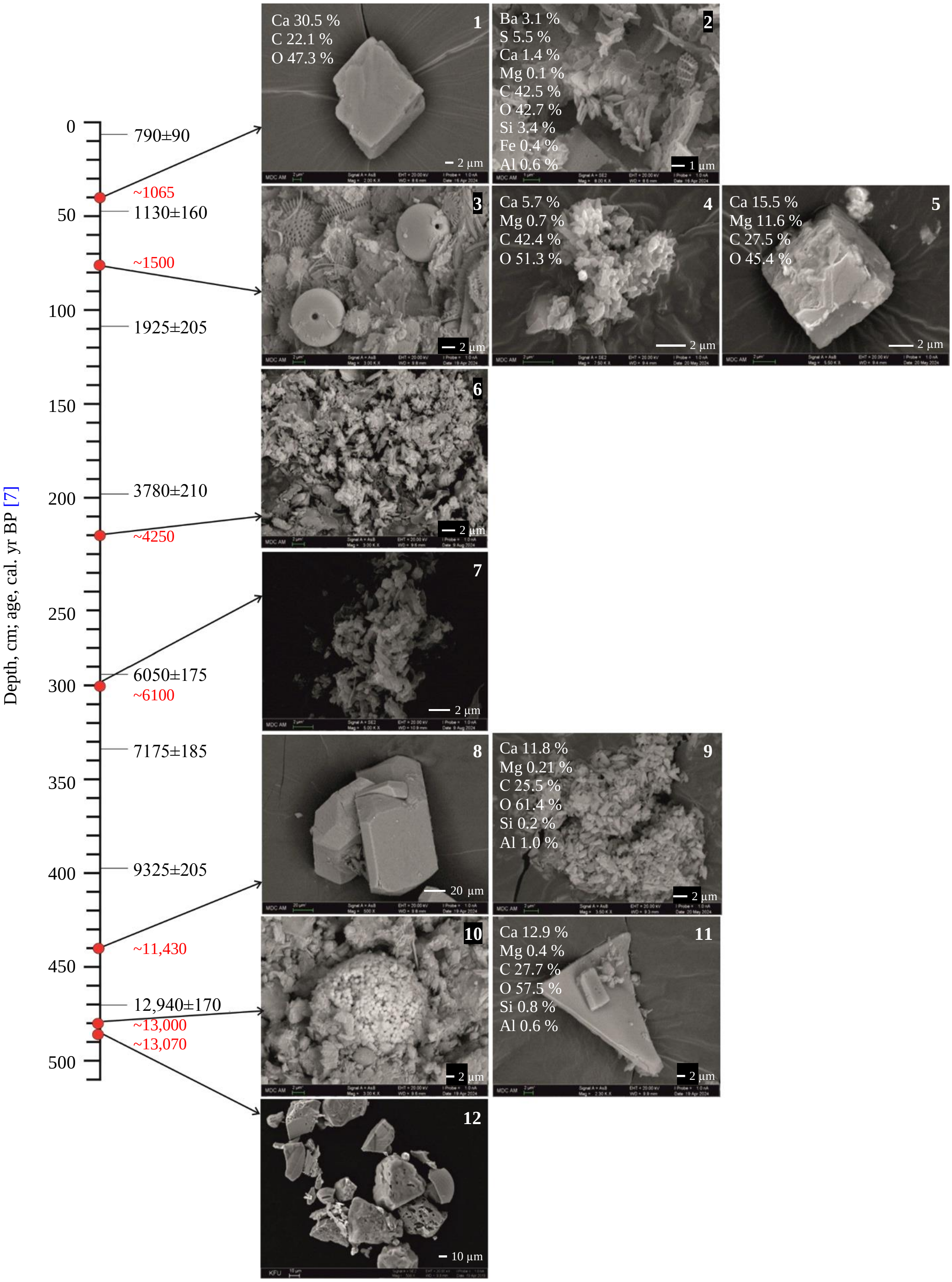


Fig.4. Scanning electron microscope images of studied samples

1, 11 – calcite; 2 – barite; 3 – biogenic silica; 4, 6, 7, 9 – aragonite; 5 – dolomite; 8 – gypsum; 10 – pyrite; 12 – iron oxides

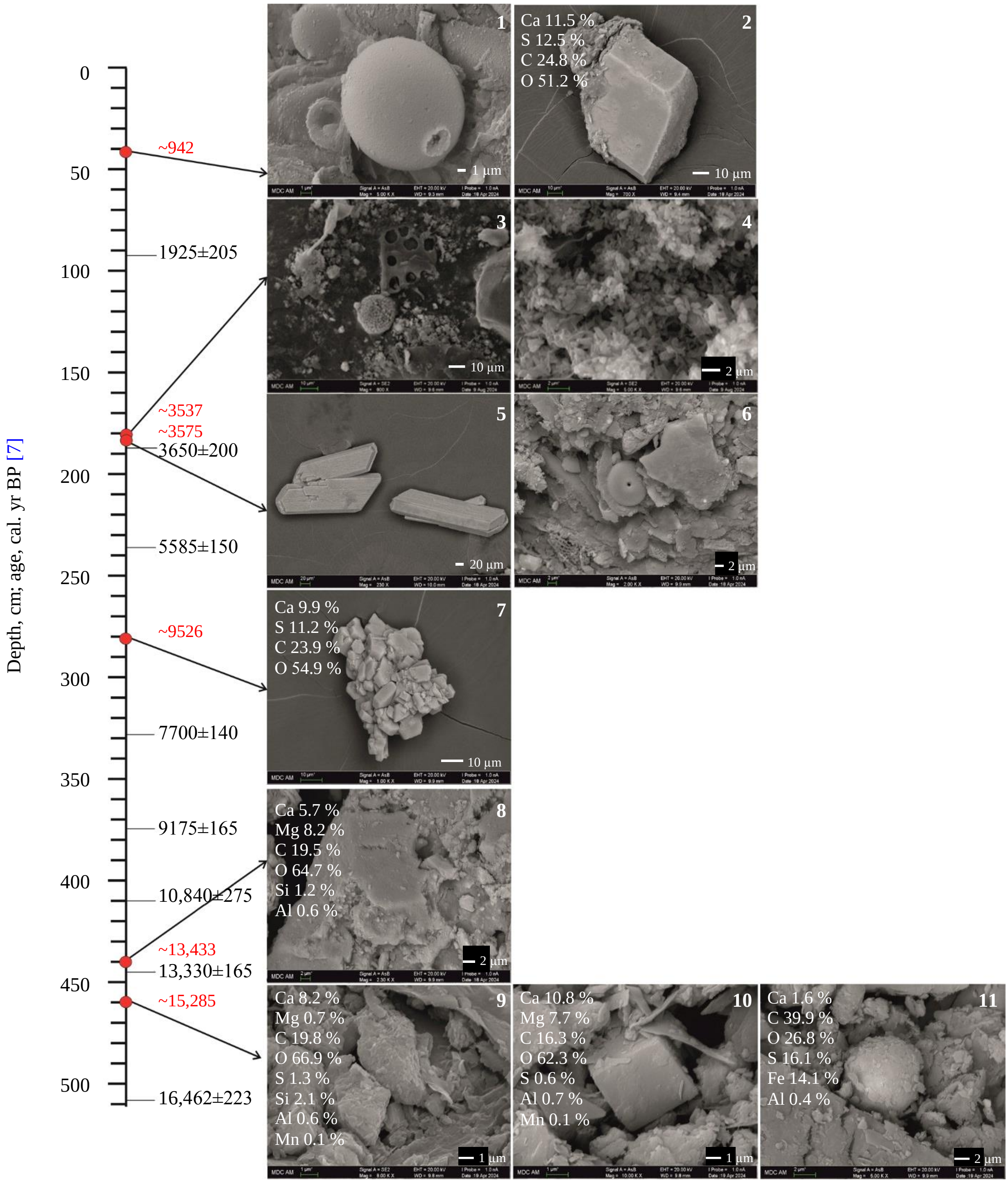


Fig.5. Scanning electron microscope images of studied samples

1, 6 – biogenic silica; 2, 5, 7 – gypsum; 3, 11 – pyrite; 4 – aragonite; 8, 10 – dolomite; 9 – calcite

Figure 6 shows the chemical compositions of the studied sediments compared with the compositions of other lakes and rocks forming the surroundings of the lakes.

Values of the ICV, which reflects the effects of recycling and sorting of sedimentary material, were calculated. Sediments from lakes Bolshoye Miassovo and Maloye Miassovo show high ICV values (> 1). This allowed us to conclude that the studied deposits represent products of primary allothigenic input [19, 20].

Journal of Mining Institute. 2026. Vol. 280. P. 47-69


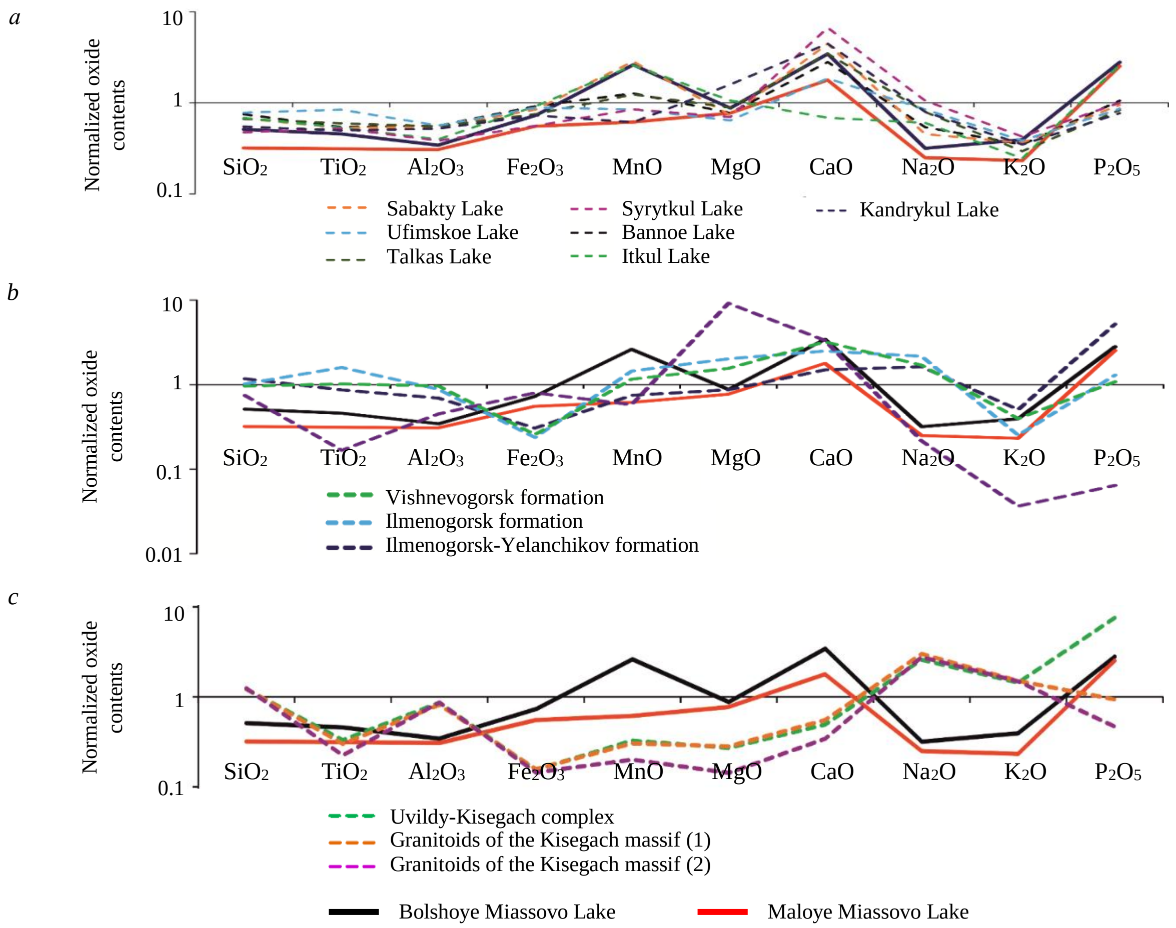


Fig.6. Comparison of the major-element compositions of sediments from lakes Bolshoye Miassovo and Maloye Miassovo with published datasets from [6, 17, 21, 22] (*a*), chemical compositions of rocks of the Vishnevogorsk and Ilmenogorsk-Yelanchikov formations, and the Baik complex after [11], and chemical composition of rocks of the Ilmenogorsk formation after [23] (*b*), chemical compositions of rocks of the Uvildy-Kisegach complex after [11], granitoids of the Kisegach massif (1) after [24], and granitoids of the Kisegach massif (2) after [23] (*c*). Normalization was performed after [20]

The results of correlation analysis for the entire dataset from Bolshoye Miassovo Lake (Table 5) and Maloye Miassovo Lake (Table 6) are presented. Spearman's rank correlation coefficients were used, pairwise deletion was applied, correlations highlighted in red are significant at $p < 0.05$ (Tables 5, 6).

*Table 5*

**Correlation matrix (Bolshoye Miassovo Lake)**

| | LOI | $Na_2O$ | MgO | $Al_2O_3$ | $SiO_2$ | $P_2O_5$ | $SO_3$ | Cl | $K_2O$ | CaO | $TiO_2$ | MnO | $Fe_2O_3$ | NiO | CuO | ZnO | $Rb_2O$ | SrO | $ZrO_2$ |
|---|---|---|---|---|---|---|---|---|---|---|---|---|---|---|---|---|---|---|---|
| LOI | **1.00** | | | | | | | | | | | | | | | | | | |
| $Na_2O$ | –0.46 | **1.00** | | | | | | | | | | | | | | | | | |
| MgO | –0.48 | 0.86 | **1.00** | | | | | | | | | | | | | | | | |
| $Al_2O_3$ | –0.34 | 0.66 | 0.82 | **1.00** | | | | | | | | | | | | | | | |
| $SiO_2$ | –0.32 | –0.38 | –0.43 | –0.55 | **1.00** | | | | | | | | | | | | | | |
| $P_2O_5$ | –0.17 | 0.44 | 0.53 | 0.30 | 0.03 | **1.00** | | | | | | | | | | | | | |
| $SO_3$ | 0.27 | 0.16 | 0.20 | 0.35 | –0.77 | –0.25 | **1.00** | | | | | | | | | | | | |
| Cl | 0.27 | –0.10 | –0.13 | –0.37 | 0.21 | 0.28 | –0.06 | **1.00** | | | | | | | | | | | |
| $K_2O$ | –0.47 | 0.81 | 0.96 | 0.88 | –0.41 | 0.49 | 0.19 | –0.20 | **1.00** | | | | | | | | | | |
| CaO | –0.61 | 0.80 | 0.80 | 0.48 | –0.18 | 0.43 | –0.06 | –0.01 | 0.73 | **1.00** | | | | | | | | | |
| $TiO_2$ | –0.49 | 0.78 | 0.94 | 0.88 | –0.40 | 0.47 | 0.19 | –0.23 | 0.98 | 0.71 | **1.00** | | | | | | | | |
| MnO | –0.56 | 0.25 | 0.31 | 0.15 | 0.10 | 0.34 | –0.13 | 0.04 | 0.22 | 0.45 | 0.25 | **1.00** | | | | | | | |
| $Fe_2O_3$ | 0.05 | 0.20 | 0.31 | 0.63 | –0.62 | 0.08 | 0.47 | –0.42 | 0.36 | –0.11 | 0.38 | 0.13 | **1.00** | | | | | | |
| NiO | –0.42 | 0.70 | 0.84 | 0.85 | –0.38 | 0.51 | 0.23 | –0.23 | 0.87 | 0.52 | 0.89 | 0.30 | 0.53 | **1.00** | | | | | |
| CuO | –0.35 | 0.53 | 0.69 | 0.80 | –0.40 | 0.23 | 0.25 | –0.54 | 0.75 | 0.36 | 0.76 | 0.12 | 0.58 | 0.75 | **1.00** | | | | |
| ZnO | –0.05 | 0.22 | 0.34 | 0.36 | –0.03 | 0.56 | –0.13 | 0.06 | 0.37 | 0.10 | 0.37 | 0.16 | 0.31 | 0.44 | 0.34 | **1.00** | | | |
| $Rb_2O$ | –0.48 | 0.68 | 0.80 | 0.74 | –0.34 | 0.35 | 0.12 | –0.22 | 0.81 | 0.70 | 0.83 | 0.32 | 0.34 | 0.75 | 0.66 | 0.26 | **1.00** | | |
| SrO | –0.65 | 0.81 | 0.83 | 0.52 | –0.16 | 0.47 | –0.05 | 0.00 | 0.77 | 0.98 | 0.75 | 0.47 | –0.07 | 0.59 | 0.40 | 0.14 | 0.73 | **1.00** | |
| $ZrO_2$ | –0.48 | 0.78 | 0.90 | 0.82 | –0.40 | 0.50 | 0.22 | –0.19 | 0.95 | 0.71 | 0.94 | 0.25 | 0.37 | 0.83 | 0.74 | 0.35 | 0.80 | 0.75 | **1.00** |

*Table 6*

**Correlation matrix (Maloye Miassovo Lake)**

| | LOI | $Na_2O$ | MgO | $Al_2O_3$ | $SiO_2$ | $P_2O_5$ | $SO_3$ | $K_2O$ | CaO | $TiO_2$ | $Cr_2O_3$ | MnO | $Fe_2O_3$ | NiO | CuO | ZnO | $Rb_2O$ | SrO | $ZrO_2$ |
|---|---|---|---|---|---|---|---|---|---|---|---|---|---|---|---|---|---|---|---|
| LOI | **1.00** | | | | | | | | | | | | | | | | | | |
| $Na_2O$ | –0.66 | **1.00** | | | | | | | | | | | | | | | | | |
| MgO | –0.78 | 0.73 | **1.00** | | | | | | | | | | | | | | | | |
| $Al_2O_3$ | –0.85 | 0.68 | 0.93 | **1.00** | | | | | | | | | | | | | | | |
| $SiO_2$ | –0.54 | 0.51 | 0.74 | 0.73 | **1.00** | | | | | | | | | | | | | | |
| $P_2O_5$ | –0.48 | 0.59 | 0.78 | 0.73 | 0.73 | **1.00** | | | | | | | | | | | | | |
| $SO_3$ | –0.38 | 0.19 | 0.24 | 0.22 | –0.25 | 0.02 | **1.00** | | | | | | | | | | | | |
| $K_2O$ | –0.84 | 0.70 | 0.93 | 0.99 | 0.72 | 0.73 | 0.23 | **1.00** | | | | | | | | | | | |
| CaO | –0.81 | 0.62 | 0.60 | 0.63 | 0.16 | 0.35 | 0.58 | 0.64 | **1.00** | | | | | | | | | | |
| $TiO_2$ | –0.75 | 0.69 | 0.95 | 0.97 | 0.82 | 0.81 | 0.10 | 0.97 | 0.51 | **1.00** | | | | | | | | | |
| $Cr_2O_3$ | –0.57 | 0.56 | 0.84 | 0.76 | 0.78 | 0.85 | 0.03 | 0.73 | 0.32 | 0.83 | **1.00** | | | | | | | | |
| MnO | –0.91 | 0.67 | 0.75 | 0.82 | 0.34 | 0.50 | 0.53 | 0.82 | 0.93 | 0.70 | 0.49 | **1.00** | | | | | | | |
| $Fe_2O_3$ | –0.58 | 0.65 | 0.88 | 0.84 | 0.80 | 0.88 | 0.02 | 0.83 | 0.34 | 0.92 | 0.84 | 0.54 | **1.00** | | | | | | |
| NiO | –0.59 | 0.64 | 0.91 | 0.84 | 0.82 | 0.90 | 0.04 | 0.83 | 0.37 | 0.92 | 0.90 | 0.56 | 0.94 | **1.00** | | | | | |
| CuO | –0.69 | 0.60 | 0.81 | 0.86 | 0.70 | 0.75 | 0.10 | 0.87 | 0.47 | 0.88 | 0.75 | 0.67 | 0.82 | 0.84 | **1.00** | | | | |
| ZnO | –0.58 | 0.61 | 0.87 | 0.84 | 0.73 | 0.90 | 0.10 | 0.84 | 0.42 | 0.89 | 0.86 | 0.61 | 0.89 | 0.94 | 0.87 | **1.00** | | | |
| $Rb_2O$ | –0.78 | 0.73 | 0.89 | 0.87 | 0.70 | 0.74 | 0.21 | 0.85 | 0.61 | 0.87 | 0.78 | 0.74 | 0.83 | 0.83 | 0.77 | 0.85 | **1.00** | | |
| SrO | –0.86 | 0.60 | 0.66 | 0.71 | 0.22 | 0.34 | 0.59 | 0.71 | 0.95 | 0.58 | 0.37 | 0.93 | 0.40 | 0.43 | 0.52 | 0.49 | 0.71 | **1.00** | |
| $ZrO_2$ | –0.77 | 0.70 | 0.92 | 0.94 | 0.66 | 0.71 | 0.27 | 0.95 | 0.66 | 0.93 | 0.71 | 0.79 | 0.83 | 0.82 | 0.80 | 0.85 | 0.90 | 0.75 | **1.00** |

*Factor analysis*. As a result of factor analysis of the geochemical dataset for Bolshoye Miassovo Lake sediments (for the retained variables), five factors (F1-F5) were identified. Each factor includes variables with significant loadings of at least 0.7 (Table 7).

From Table 7 it can be seen that, for Bolshoye Miassovo Lake, factor F1 explains the largest share of the total variance (0.33) and is associated with increased contents of Ti, K, Mg, Ni, and Zr. Biogenic-chemogenic particles are represented by biogenic silica, carbonates, sulfates, and sulfides (see Fig.4, 5). Their contribution is reflected in the structure of factors F2-F5 (Table 7). For Bolshoye Miassovo Lake, these factors indicate pyrite crystallization (F2), carbonate formation (F3), Br accumulation (F4) as an indicator of Holocene warming [25], and Cl accumulation (F5) – chlorine may originate from rocks containing small inclusions of chloride salts in pores and fractures (Table 7). Factor F2 accounts for 0.19 of the total variance and has a bipolar structure. On one pole it reflects increasing Fe and S contents, and on the other pole it reflects decreasing Si. Factor F3 accounts for 0.13 of the total variance and is associated with increased Ca and Sr contents. Factor F4 (0.09 of the total variance) and factor F5 (0.08 of the total variance) are the bromine and chlorine factors, respectively.

For sediments of Lake Maloye Miassovo, the largest share of the total variance (0.48) is explained by factor F1 (Table 7). Factor F1 has a bipolar structure: on one pole it correlates with increasing contents of allothigenic elements Si, Ti, Al, Cr, K, Ni, Mg, Cu, Zn, Fe, Rb, and Zr, and on the other pole it reflects decreasing organic-matter content (LOI). Factor F2, which explains 0.21 of the total variance, reflects increasing Ca, Sr, and S contents. Factor F3 (0.06 of the total variance) correlates with increasing Cl contents. Factor F4 is associated with increasing Br contents (0.06 of the total variance). These factors are analogous to factors F5 and F4 for Bolshoye Miassovo Lake. Factor F5 (0.06 of the total variance) reflects increasing phosphorus contents.

*Coercivity spectrometry*. For Bolshoye Miassovo Lake, total magnetic susceptibility (k_full) ranges within (2.16-52.16)$\cdot 10^{-5}$, k_para ranges within (1.81-8.33)$\cdot 10^{-5}$, k_ferro ranges from $0.24\cdot 10^{-5}$ to $42.61\cdot 10^{-5}$ and k_super ranges from $0.001\cdot 10^{-5}$ to $1.35\cdot 10^{-5}$. For Maloye Miassovo Lake, k_full ranges from (1.31-22.31)$\cdot 10^{-5}$, k_para ranges from (0.29-8.78)$\cdot 10^{-5}$, k_ferro ranges from $0.03\cdot 10^{-5}$ to $15.41\cdot 10^{-5}$ and k_super ranges within $0.001\cdot 10^{-5}$ to $0.41\cdot 10^{-5}$. A strong positive relationship between k_para and factor F1 was found for both lakes (correlation coefficient 0.65 for Bolshoye Miassovo Lake sediments and 0.79 for Maloye Miassovo Lake sediments).

Late Pleistocene sediments of Bolshoye Miassovo Lake (depth interval 528-480 cm, ~13,400-13,000 cal. yr BP), represented by sandy loam and silty sandy loam, show reduced k_para values. The end of the Late Pleistocene (depth interval 480-448 cm, ~13,000-11,700 cal. yr BP) is characterized

***Journal of Mining Institute.*** *2026. Vol. 280. P. 47-69*


by increased k_para values. During the interval 480-304 cm (~11,700-6200 cal. yr BP), k_para varies within (2.02-4.95)·$10^{-5}$. During the Subboreal stage, k_para and factor F1 decrease sharply, whereas Md increases at 242 cm (~ 4752 cal. yr BP).

*Table 7*

**Results of factor analysis of sediments of lakes Bolshoye Miassovo and Maloye Miassovo**

| Component | F1 | F2 | F3 | F4 | F5 |
|---|---|---|---|---|---|
| Bolshoye Miassovo Lake | | | | | |
| Mg | 0.83 | 0.18 | 0.33 | 0.21 | 0.15 |
| Si | –0.21 | –0.5 | –0.07 | –0.11 | –0.02 |
| P | 0.46 | 0.05 | 0.23 | 0.22 | 0.12 |
| Cl | 0.12 | –0.05 | 0.26 | 0.09 | 0.95 |
| K | 0.91 | 0.17 | 0.21 | 0.18 | 0.10 |
| Ti | 0.94 | 0.19 | 0.13 | 0.13 | 0.05 |
| Ni | 0.79 | 0.31 | 0.02 | 0.01 | 0.00 |
| Fe | 0.20 | 0.83 | –0.38 | –0.16 | –0.18 |
| Br | 0.32 | 0.07 | 0.30 | 0.87 | 0.11 |
| Rb | 0.59 | 0.07 | 0.28 | 0.08 | 0.14 |
| Sr | 0.40 | –0.22 | 0.73 | 0.30 | 0.29 |
| Zr | 0.75 | 0.19 | 0.18 | 0.33 | 0.11 |
| S | 0.20 | 0.95 | –0.11 | 0.11 | 0.02 |
| Ca | 0.29 | –0.24 | 0.83 | 0.21 | 0.27 |
| Total variance | 4.64 | 2.67 | 1.89 | 1.20 | 1.17 |
| Share of total variance | 0.33 | 0.19 | 0.13 | 0.09 | 0.08 |
| Maloye Miassovo Lake | | | | | |
| LOI | –0.88 | –0.36 | –0.06 | –0.09 | –0.16 |
| Na | 0.32 | 0.31 | 0.05 | 0.15 | 0.13 |
| Mg | 0.82 | 0.46 | 0.14 | 0.16 | 0.11 |
| Al | 0.89 | 0.34 | 0.11 | 0.11 | 0.16 |
| Si | 0.85 | –0.06 | –0.11 | 0.13 | 0.08 |
| P | 0.45 | 0.16 | 0.22 | 0.07 | 0.83 |
| Cl | 0.11 | 0.36 | 0.91 | 0.02 | 0.17 |
| K | 0.87 | 0.38 | 0.11 | 0.11 | 0.17 |
| Ca | 0.26 | 0.87 | 0.16 | 0.01 | 0.24 |
| Ti | 0.90 | 0.32 | 0.05 | 0.14 | 0.17 |
| Cr | 0.85 | 0.20 | 0.13 | 0.09 | 0.25 |
| Mn | 0.64 | 0.65 | 0.16 | –0.14 | 0.22 |
| Fe | 0.85 | 0.31 | 0.04 | 0.10 | 0.20 |
| Ni | 0.82 | 0.37 | 0.19 | 0.15 | 0.26 |
| Zn | 0.73 | 0.25 | 0.30 | 0.11 | 0.18 |
| Br | 0.25 | 0.00 | 0.02 | 0.96 | 0.05 |
| Rb | 0.75 | 0.49 | 0.10 | 0.24 | 0.01 |
| Sr | 0.47 | 0.80 | 0.21 | 0.19 | –0.04 |
| Zr | 0.75 | 0.56 | 0.08 | 0.22 | –0.01 |
| S | 0.25 | 0.82 | 0.28 | –0.13 | 0.05 |
| Cu | 0.74 | 0.00 | 0.30 | 0.15 | 0.18 |
| Total variance | 9.98 | 4.33 | 1.36 | 1.30 | 1.21 |
| Share of total variance | 0.48 | 0.21 | 0.06 | 0.06 | 0.06 |

Late Pleistocene sediments of Maloye Miassovo Lake (depth interval 512-454 cm, ~ 20,100-14,700 cal. yr BP) are characterized by low k_para values. The subsequent warm Bølling stage 454-448 cm, ~14,700-14,100 cal. yr BP) is accompanied by a sharp increase in k_para; values then vary within a narrow range from 5.59·$10^{-5}$ to 6.92·$10^{-5}$ until the beginning of the Holocene. The Preboreal and Boreal stages (depth interval 422-398 cm, ~11,700-10,200 cal. yr BP) show a decreasing trend in k_para, indicating reduced input of allothigenic material. At the same time, LOI increases, indicating higher organic-matter content in the sediment. The beginning of the Atlantic stage (depth interval 354-346 cm, ~ 8500-8200 cal. yr BP) is marked by a sharp increase in k_para and factor F1, together with a sharp decrease in LOI. In addition to the events described above, the Subatlantic stage is characterized by a sharp decrease in k_para and factor F1, and by a sharp increase in Md and in the proportion of the psammitic fraction at 104 cm (~ 2100 cal. yr BP). This depth is also characterized by increased LOI and increased biogenic-silica content.

**Discussion**

Based on grain-size data and mineralogical and chemical composition, the studied lacustrine sediments show a pattern typical of freshwater lakes: the predominance of allothigenic particles in the silt-size range.

Comparison of the geochemical composition of sediments from the studied lakes with that of the other lakes of the Southern Urals shows the expected regional similarity (Fig.6, *a*). Distinctive features include higher MnO and CaO contents in sediments of Bolshoye Miassovo Lake. These values reflect a substantial presence of authigenic carbonates and evaporites in the sediment (see Fig.4). In contrast, sediments of Maloye Miassovo Lake have higher $P_2O_5$ contents, which is linked to the occurrence of phosphorite-bearing rocks within the lake basin (see Fig.1).

Analysis of geological maps of pre-Quaternary bedrock and Quaternary deposits (see Fig.1) indicates that the main source of allothigenic material for the studied lakes is Quaternary deposits. These deposits are represented by eluvial, slopewash, colluvial, and alluvial facies. As expected, they consist of clasts of mature mineral components such as quartz, feldspars, clay minerals, and iron oxides. In the west, Quaternary deposits are only a few meters thick, whereas around the rest of the lakes their thickness can reach up to 20 m. Therefore, when deep channel incisions develop from the west, material may enter the lake as a result of erosion not only of Quaternary deposits but also of pre-Quaternary bedrock. In the western sector, erosion may primarily affect the Ilmenogorsk formation, the Yelanchikov formation, and the Baik complex (see Fig.1). Figure 6, *b* compares the chemical composition of rocks from these formations with that of the lake sediments.

On the western shore of Bolshoye Miassovo Lake, amphibolites of the Ilmenogorsk formation crop out. Compared with amphibolites of the Kyshtym formation, which occur farther east, these amphibolites are characterized by lower Na contents and slightly lower Ca and Fe contents. The low $Na_2O$ contents in sediments of the studied lakes (Fig.6, *b*) are likely related to leaching of amphibolites of the Ilmenogorsk formation, as well as leaching of mafic and ultramafic rocks of the Ilmenogorsk complex and igneous rocks of the Ilmensky Mountains [26].

The eastern shore of Bolshoye Miassovo Lake is composed of granitoids of the Kisegach massif. A comparative plot of major elements for lakes Bolshoye Miassovo and Maloye Miassovo and the chemical composition of rocks of the Kisegach massif is shown in Fig.6, *c* [24]. Rocks of the Kisegach massif are represented mainly by leucogranites, which locally contain small xenoliths of granosyenites, granodiorites, and adamellites. The comparative plots (Fig.6) show that the chemical composition of sediments from the studied lakes is less similar to the composition of rocks of the Uvildy-Kisegach complex and to granitoids of the Kisegach massif (Fig.6, *c*). This suggests that allothigenic material was supplied not directly from the Uvildy-Kisegach complex and the Kisegach massif, but from the Quaternary deposits that overlie them. On the eastern side of the lakes, these Quaternary deposits are thicker than on the western side (see Fig.1).

Based on ICV values and A-CN-K diagrams [19, 20], the sediments of the studied lakes formed predominantly from stable allothigenic minerals of the primary sedimentation cycle, sourced mainly from Quaternary deposits and exposed pre-Quaternary rocks. The transport pathways of allothigenic material are linked to the directions of slope flows and channel networks visible on the Quaternary-deposit map (see Fig.1).

Based on correlation matrix for Bolshoye Miassovo Lake, Si, among the major elements, shows a pronounced negative correlation with Al, Fe, and S (see Table 5). At the same time, Si shows no correlation with Ti, Mg, K, or Na. This pattern suggests that a substantial fraction of Si is hosted in quartz grains, while another substantial fraction is associated with biogenic silica. This interpretation is generally supported by scanning electron microscopy (see Fig.4, image 3). Al shows positive correlations with K, Ti, Fe, Ni, Cu, Rb, Sr, and Zr. This allows us to infer the presence of feldspars, montmorillonite, rutile, anatase, iron oxides, nickel sulfides, and zircons. Indeed, aluminosilicate minerals such as feldspars and montmorillonite clays show a positive relationship between Al and K, as well as with other cations, for example Ti [27]. In titanium oxides (rutile and anatase), Ti can be substituted by Al in the crystal lattice. Hematite and magnetite are Fe-bearing minerals in which Fe can be isomorphically substituted by Al [28]. In nickel sulfides, the association of Ni and Fe with Al can reflect their common magmatic source. In zircons, a positive correlation between Zr and Al may occur due to structural substitutions [29]. Rb belongs to the alkali-element group and can substitute for K in the structures of feldspars or montmorillonite. A positive correlation of Rb with Al has been reported for alkaline silicate rocks [30].

The mineralogical inferences based on chemistry are supported by X-ray diffraction data (XRD) (see Table 3, Fig.3), which revealed feldspars, mixed-layer clays, and other clay minerals in substantial amounts. Other minerals (hematite, magnetite, nickel sulfides, zircons) are not detected by XRD because their contents are below 2 % and they occur as accessory phases. A positive correlation of Na with Mg, K, Ca, and Ti is typical for a number of mineral groups. For example, in nepheline-bearing silicates, Na content is closely related to the presence of K, Ca, and Mg [31]. In Na-Mg silicates, Na often substitutes for K or Mg in structural sites [32]. In leucoxenes or rutile, Ti content can correlate with Na [33]. In sodium-calcium carbonates, Na content is linked to Ca through exchange processes [34]. Positive relationships of Mg with K, Ca, Ti, and P may indicate the presence of magnesian carbonates and phosphates [35]. For example, magnesium hydrogen phosphate (magnesium phosphate) contains substantial Mg associated with the phosphate group. In Ti- and K-rich pegmatites, minerals with elevated Mg contents are often found. [36]. In olivines, Mg content is related to Ca and sometimes to K in cases of structural substitution [37]. In natural olivines, Mg often correlates with Ti due to inclusions or substitutions in the structure [38]. LOI shows a negative correlation with Ca, Mn, and Sr. This indicates an inverse relationship between carbonate material and organic matter. Organic matter in sediments decomposes upon heating and causes substantial mass loss. Therefore, higher organic-matter content results in higher LOI. In clay-rich sedimentary deposits, organic matter is associated with humic substances, organic remains, or hydrated compounds. In carbonate deposits, mass loss is also related to the decomposition of $CaCO_3$, while the proportion of organic matter decreases [39]. The pattern of correlations for Maloye Miassovo Lake (see Table 6) may be controlled by several mineral groups: the (Si, Al, Ti, Zr, K, Mg, Fe) association may reflect silicate minerals (quartz, opal, clay minerals); the (Al, Si, K, Mg, Fe) association may reflect clay minerals (kaolinite, illite, smectite); the P-Ca association may reflect phosphate minerals (apatite); the (Fe, S, Cu) association may reflect sulfates and sulfides; Fe alone may reflect hematite and magnetite; the (Zr, Si) association may reflect zircons; and the (Mg, Ca) association may reflect magnesite and dolomite [40, 41]. The negative correlation of LOI with all elements indicates that, as in Bolshoye Miassovo Lake, LOI is associated with hydrated and/or organic components that readily decompose upon heating.

According to the factor analysis for Bolshoye Miassovo Lake (Table 7), factor F1 explains the largest share of the total variance and is associated with increased Ti, K, Mg, Ni, and Zr contents. The most likely candidates responsible for a simultaneous increase in Ti, K, Mg, Ni, and Zr-either as trace admixtures or through isomorphism are K-feldspars (minerals derived from sedimentary rocks); garnets and zircon (igneous minerals); titanomagnetite (a magnetic mineral formed during metasomatism); hornblende, and sulfides of hydrothermal ores [40]. The influence of factor F2 can be explained as follows. In lacustrine bottom sediments, decreasing Eh-among other reasons due to decomposition of organic matteroften activates bacterial sulfate reduction. This process reduces Fe(III) to Fe(II), which is readily precipitated as hydrogenic hydrates or sulfides (e.g., pyrite). In lake sediments, Si is largely represented by diatom remains (silica), which precipitate actively under favorable conditions. Under acidic or alkaline conditions, diatom skeletons may dissolve or decompose due to bacterial activity. When Eh decreases, silica dissolution can intensify due to the formation of soluble Si species. Thus, increasing Fe and S may be related to post-sedimentary formation of hydrogenic sulfides, whereas decreasing Si may reflect dissolution of diatom remains under changed environmental conditions [40, 41]. Factor F3 is associated with increased Ca and Sr contents. Calcium and strontium have similar chemical properties because both are alkaline-earth elements and form analogous compounds, for example carbonates ($CaCO_3$ and $SrCO_3$). Strontium often enters Ca-bearing minerals such as calcite ($CaCO_3$), which promotes their joint supply and accumulation in sediments. Inputs of Ca and Sr from surrounding rocks affect their concentrations in lake water. For example, weathering of limestones or dolomites increases the concentrations of these elements in the lake. In regions where limestones and dolomites are common, Ca and Sr levels increase in water and, consequently, in bottom sediments.

Climate change can influence the chemical balance of lakes. Higher humidity promotes leaching of elements from soils and rocks, whereas temperature changes affect biological activity and sedimentation rates. This can lead to a simultaneous increase in Ca and Sr concentrations [21]. Factors F4 and F5 are the bromine and chlorine factors, respectively. In freshwater lakes, exchange with the surrounding environment can lead to accumulation of Cl and Br through infiltration of water from surrounding soils and rocks. Decomposition of organic matter and biogeochemical cycles can contribute to the mobilization and redistribution of Br and Cl within the lake [42].

For Maloye Miassovo Lake, the factor analysis (Table 7), shows that factor F1 is associated with increased contents of allothigenic elements Si, Ti, Al, Cr, K, Ni, Mg, Cu, Zn, Fe, Rb, and Zr, and with decreased organic-matter content (LOI). This pattern reflects an increase in stable minerals (hematite, quartz, feldspars, zircon, kaolinite, chlorite, and hornblende) and a decrease in hydrated clays and organic matter [40, 41]. Factor F2 reflects increasing Ca, Sr, and S contents and is similar to factor F3 for Bolshoye Miassovo Lake (the coupled increase in Ca and Sr). The difference for Maloye Miassovo Lake is the additional element S. This structure can be explained by the simultaneous formation of carbonate and sulfate minerals in Maloye Miassovo Lake sediments. Factors F3 and F4 are analogous to factors F5 and F4, respectively, for Bolshoye Miassovo Lake. Factor F5 reflects increasing phosphorus contents, which may indicate changes in the ecological state of the lake, intensified eutrophication, or changes in input sources.

The main sources of phosphorus are organic and inorganic substances delivered by water masses through weathering of bedrock, river runoff, agricultural and industrial waste, and atmospheric deposition. In aquatic environments, phosphorus is readily bound to suspended particles and to the biomass of microorganisms, plants, and animals. After their death and decomposition, phosphorus becomes incorporated into bottom sediments. Under low dissolved-oxygen conditions, phosphate minerals precipitate (e.g., apatite, $Ca_5(PO_4)_3(OH, F, Cl)$. The hydrogen parameter also affects phosphate solubility: under neutral to alkaline conditions, phosphates tend to precipitate. Concentrations of Fe(III) and Al(III) are also important because, upon oxidation, they bind phosphate ions and form insoluble compounds [43]. Given the consistent relationship between factor F1 and k_para in both lakes, k_para can be treated as an indicator of allothigenic material supply to the lacustrine basin, as has also been shown for other lakes [17, 21].

Grain-size, mineralogical, and chemical data are presented as variations of the main indicators and are compared with global and regional climatic stages and events (Fig.7).

*Late Pleistocene*. The Last Glacial Maximum represents the period of maximum cooling during the last glaciation. During this interval (between ~27,000 and ~19,000 cal. yr BP), global ice sheets reached their maximum integrated volume [44, 45]. In Fig.7, *b*, this episode is represented by a small number of observations. These points mark the beginning of a coherent trend of decreasing k_para and decreasing allothigenic-mineral content that continues through the Early Dryas to ~16,000 cal. yr BP. This trend indicates reduced delivery of allothigenic material to the sedimentation basin, likely associated with the cold and dry conditions of the last glaciation. At the same time, gypsum contents are high and appear to be largely diagenetic. The warming that followed the last glaciation occurred at ~14,700 cal. yr BP and marked the onset of the Bølling climatic stage [43]. Warming and increased moisture were accompanied by higher k_para values, indicating enhanced delivery of allothigenic material to the sedimentation basin of Maloye Miassovo Lake (Fig.7, *b*). During ~13,000-11,700 cal. yr BP, sediments of both lakes Bolshoye Miassovo and Maloye Miassovo show increased k_para values and higher allothigenic-mineral contents. This reflects enhanced allothigenic

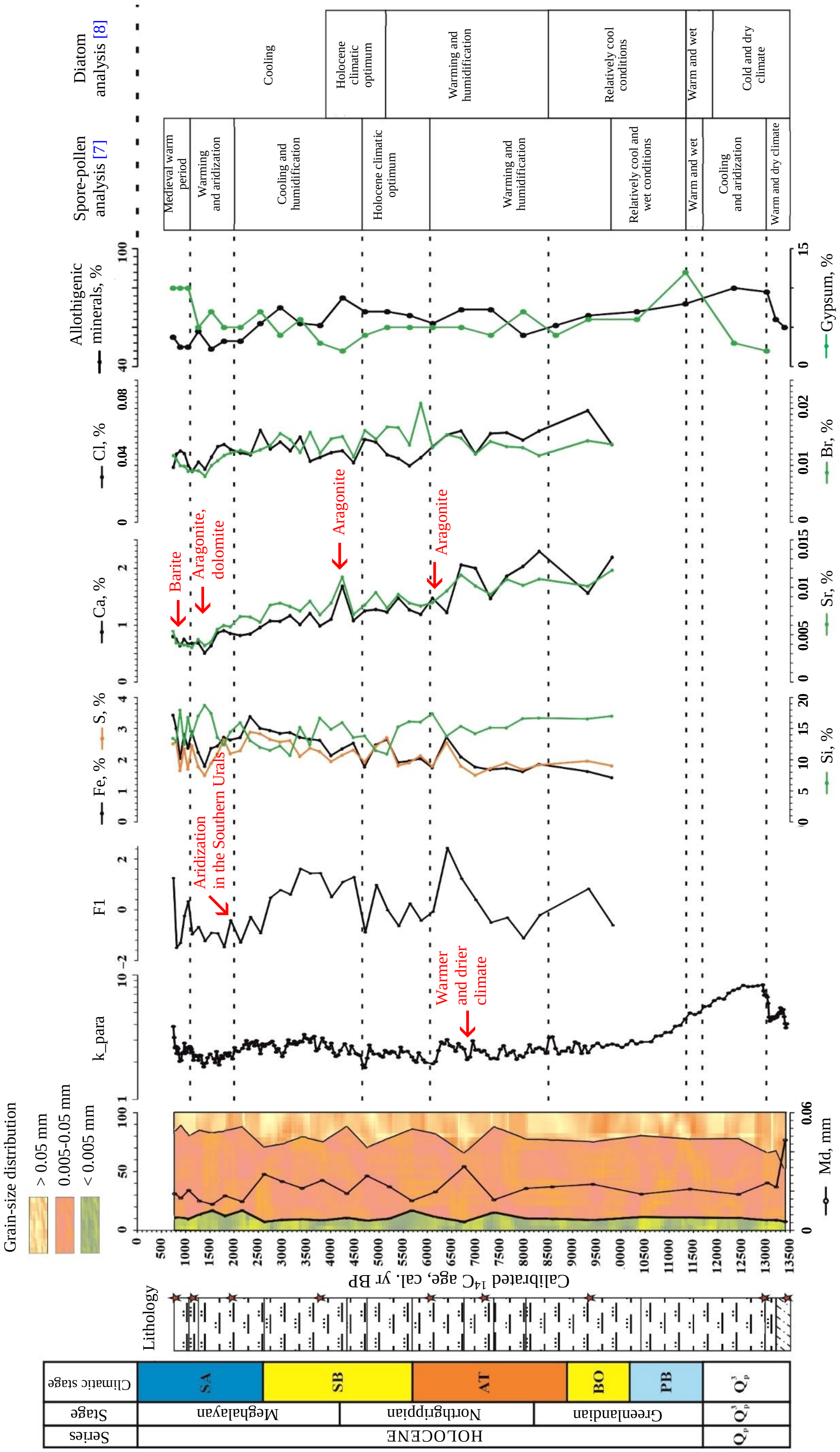
Series
Stage
Climatic stage
HOLOCENE
Meghalayan
Northgrippian
Greenlandian
SA
SB
AT
BO
PB
Lithology
Calibrated 14C age, cal. yr BP
Grain-size distribution
> 0.05 mm
0.005-0.05 mm
< 0.005 mm
Md, mm
k_para
F1
Fe, %
S, %
Si, %
Ca, %
Sr, %
Cl, %
Br, %
Allothigenic minerals, %
Gypsum, %
Spore-pollen analysis [7]
Diatom analysis [8]
Barite
Aragonite, dolomite
Aragonite
Aragonite
Aridization in the Southern Urals
Warmer and drier climate
Medieval warm period
Warming and aridization
Cooling and humidification
Holocene climatic optimum
Warming and humidification
Relatively cool and wet conditions
Warm and wet
Cooling and aridization
Warm and dry climate
Cooling
Holocene climatic optimum
Warming and humidification
Relatively cool conditions
Warm and wet
Cold and dry climate

*a*

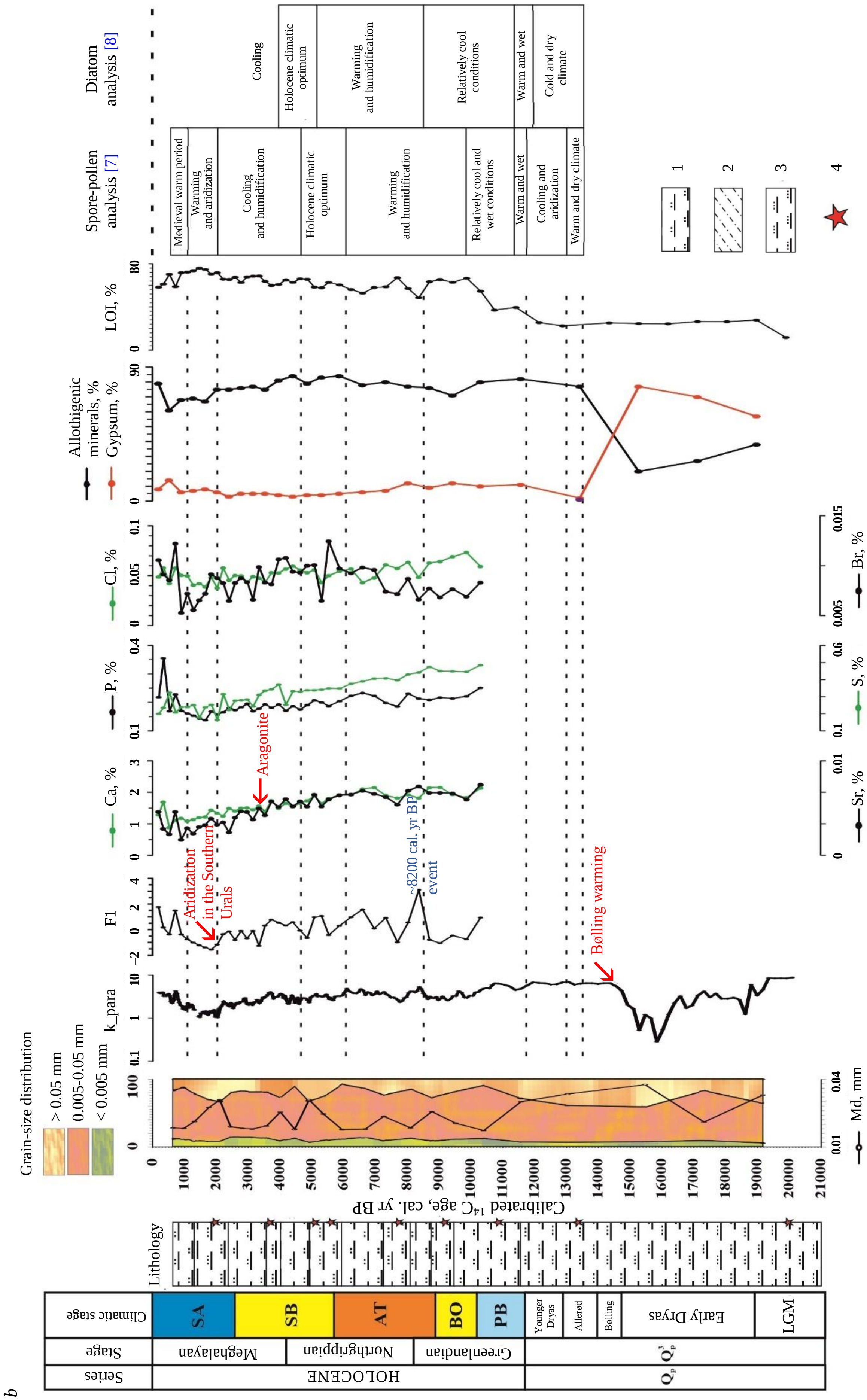


Fig.7. Results of integrated analysis of sediments from lakes Bolshoye Miassovo (*a*) and Maloye Miassovo (*b*)
1 – light silty loam; 2 – sandy loam; 3 – silty sandy loam; 4 – dated samples

input (products of erosion of rocks of the Ilmenogorsk and Yelanchikov formations and the Baik complex). The dominance of the allothigenic component together with low organic-matter contents (mean LOI ~ 23.85 %, Fig.7, *b*), indicates low productivity of the lake ecosystem under cold climatic conditions, according to [46]. Consistently, study [7] showed that during the Late Glacial (~13,200-11,700 cal. yr BP) Bolshoye Miassovo Lake was a deep-water basin with a stable water level and an extensive shallow-water zone overgrown with macrophytes under cool climatic conditions.

*Holocene*. With the onset of the Holocene (~11,700-8500 cal. yr BP), organic-matter content in the sediment increases sharply. This increase is likely related to the shift from the cold Pleistocene climate to the warmer Holocene climate. This interval is also characterized by increasing Br and Cl trends. At ~11,430 cal. yr BP, aragonite was identified in Bolshoye Miassovo Lake sediments (see Fig.4, image 9). This suggests that the lake was shallow and more mineralized during this time due to climate aridization, possibly including the global Bond Event 8 (~11,100 cal. yr BP) [47]. Maloye Miassovo Lake also shows a decreasing trend in k_para and allothigenic-mineral contents, while LOI increases. A similar trend is reported for Sabakty Lake (Southern Urals) [46], where early Holocene organic-matter accumulation and reduced allothigenic input were explained by increased lake productivity and/or soil formation in the catchment under continuing climate warming.

According to diatom analysis [8], during ~ 8500-4600 cal. yr BP Bolshoye Miassovo Lake was deep-water. This likely reflects a longer and warmer growing season, which led to complete melting of the Ural glaciers. Our results show that at ~8500 cal. yr BP the sediment-core record from Bolshoye Miassovo Lake exhibits a sharp change in k_para, factor F1, LOI, and Ca and Sr contents. This change is likely related to the global cooling event at ~8200 cal. yr BP [46]. The ~8200 cal. yr BP cooling event is reflected in numerous paleorecords from lacustrine and marine sediments and from cave speleothems in both the Northern and Southern hemispheres [48, 49]. The temperature decline is commonly attributed to the influx of large volumes of freshwater into the North Atlantic due to ice-sheet collapse and glacier melting. In Maloye Miassovo Lake, this event is accompanied by a sharp increase in k_para and factor F1 and a sharp decrease in LOI. Study [46] reports a sharp decrease in electrical conductivity in sediments of Sabakty Lake during ~8200-7700 cal. yr BP, which also corresponds to the ~8200 cal. yr BP event.

Subsequently, until ~ 7000 cal. yr BP, k_para, factor F1, and Md decrease, whereas LOI increases. This pattern may indicate subsidence of the pelagic zone due to neotectonic processes. During the same period, Maloye Miassovo Lake also shows decreases in k_para, factor F1, and in the contents of Ca, Sr, P, S, and Cl. Two events characterized by abrupt changes in k_para are distinguished. The first occurred at ~ 6760 cal. yr BP and is accompanied by an increase in Md to ~ 0.033 mm as well as increased Ca and Sr contents in the sediment. The second occurred at ~ 6100 cal. yr BP, when Ca and Sr contents increased and the presence of aragonite was recorded (see Fig.4). These events are most likely related to climatic warming and reduced humidity. For example, accumulation of laminated sapropel in Sabakty Lake during ~ 7900-6000 cal. yr BP, with high organic-matter and carbonate contents and low concentrations of allothigenic elements, indicates enhanced lake productivity, likely in response to warming [46]. For Bolshoye Miassovo Lake sediments during ~ 7000-6000 cal. yr BP, factor F1, Cl, Fe, and Md increase sharply, indicating enhanced allothigenic input to the sedimentation basin. At the same time, Ca, Sr, Si, and LOI decrease sharply. During the same interval, Maloye Miassovo Lake also shows higher values of indicators of allothigenic input, reflecting increased delivery of allothigenic material to the sedimentation basin. Notably, at ~ 6100 cal. yr BP in Bolshoye Miassovo Lake sediments, Ca and Sr increase sharply, while the indicators of allothigenic input decrease (Fig.7, *a*). This pattern likely reflects climate aridization, which is supported by the occurrence of aragonite in the sediments (see Fig.4, 5).

Elevated LOI and Br values characterize the interval ~ 6000-4700 cal. yr BP in Bolshoye Miassovo Lake sediments. This most likely reflects warm climatic conditions consistent with the Holocene climatic optimum identified in [7]. Maloye Miassovo Lake sediments during this interval are characterized by elevated Ca, Sr, and Br contents.

The interval ~ 4700-2000 cal. yr BP is characterized by increasing k_para and factor F1 values, which can be explained by increased climatic humidity and is consistent with [7]. However, the same study [7] indicates climate cooling during this period, which is supported by a decreasing trend in Ca and Sr contents in the sediments. At the same time, scanning electron microscopy identified aragonite in Bolshoye Miassovo Lake sediments at ~ 4250 cal. yr BP (see Fig.4, image 6), and sediments of Bannoe Lake (Southern Urals) show an increase in $\delta^{18}O$ [17]. In addition, aragonite was also identified in Maloye Miassovo Lake sediments at ~ 3540 cal. yr BP, consistent with data from lakes Sabakty and Talkas [6, 21]. Thus, this interval requires additional investigation.

According to [7], during ~ 2500 to ~ 800 cal. yr BP, against a background of decreasing temperature, Bolshoye Miassovo Lake ultimately formed as a deep-water basin with low-mineralized water and with boggy shallow-water zones where acidification processes occurred. Our data show that at ~2000 cal. yr BP Bolshoye Miassovo Lake sediments exhibit a sharp decrease in k_para, factor F1, Fe, Cl, and in the content of allothigenic minerals. This pattern is most likely related to climate aridization, which has been reported in multiple studies of lakes sediments in the Southern Urals [6, 7, 21]. In addition, aragonite and dolomite were identified in a Bolshoye Miassovo Lake sample at ~1500 cal. yr BP (see Fig.4, images 4, 5). This occurrence is linked to the global Bond Event 1, which manifested as aridization in the Southern Urals. Maloye Miassovo Lake sediments also show a sharp decrease in indicators of allothigenic input and in Cl and P contents, indicating reduced delivery of allothigenic material to the sedimentation basin.

**Conclusion**

Based on radiocarbon dating and grain-size, mineralogical, and geochemical analyses of bottom sediments from lakes Bolshoye Miassovo and Maloye Miassovo, we identified key features of the material composition of the studied lacustrine sediments and reconstructed lacustrine sedimentation conditions during the Late Quaternary.

The sediment core from Bolshoye Miassovo Lake consists predominantly of interbedded light silty loam and silty sandy loam. The lower part of the core is represented by sandy loam. The sediment sequence of Maloye Miassovo Lake is represented by interbedded light silty loam and silty sandy loam.

X-ray diffraction analysis showed that sediments from the studied lakes are characterized by a predominance of allothigenic minerals. Biogenic-chemogenic particles are represented by biogenic silica, carbonates, sulfates, and sulfides.

We obtained data on the contents of major and trace elements in bottom sediments of the studied lakes. Comparative plots of major-element contents for the lake sediments of the Southern Urals show that deposits from Bolshoye Miassovo Lake are characterized by higher MnO and CaO contents, which is explained by a substantial presence of authigenic carbonates and evaporites in the sediment. In sediments of Maloye Miassovo Lake, $P_2O_5$ contents are higher, which is linked to the occurrence of phosphorite-bearing rocks within the lake basin.

Variations in the most informative indicators identified from grain-size, mineralogical, and geochemical data (factor analysis) were compared with global and regional climatic stages and events. Based on the sediment records from lakes Bolshoye Miassovo and Maloye Miassovo, we identify the Bølling warming, the ~ 8200 cal. yr BP event (cooling), aridization in the Southern Urals (~ 2000 cal. yr BP), and Bond Event 1 (~1500 cal. yr BP). In addition, aragonite – an indicator of reduced climatic humidity – was recorded at ~11,430, ~6100, ~4250, and ~3540 cal. yr BP. The presence of barite at ~1065 cal. yr BP also supports the inference of climate aridization.

**REFERENCES**

1. Ekoa Bessa A.Z., Richards K., Egbe A.M., Ambo F.B. A geochemical and palynological study of lake sediments at Mboandong, Cameroon: Chemical weathering and vegetation linked to Holocene palaeoclimate. *Journal of African Earth Sciences*. 2025. Vol. 223. N 105512. DOI: 10.1016/j.jafrearsci.2024.105512

2. Subetto D.A., Rybalko A.E., Naumenko M.A. et al. The Geology, Geomorphology, and History of Lake Ladoga: A Review. *Doklady Earth Sciences*. 2024. Vol. 519. Suppl. 1, p. S91-S109. DOI: 10.1134/S1028334X24604735

3. Rybalko A.E., Repkina T.Yu., Starovoitov A.V. et al. The Main Stages in Studying Quaternary Deposits of the White Sea and Controversial Problems of Its Late Pleistocene and Holocene Paleogeography. *Izvestiya Rossiiskoi akademii nauk. Seriya Geograficheskaya.* 2022. Vol. 86. N 6, p. 848-869 (in Russian). DOI: 10.31857/S2587556622060152

4. Hongpan Xue, Xin Zhou, Luyao Tu et al. Climate-vegetation-erosion interactions revealed by the sediments of Huguangyan Maar Lake, southern China. *Catena*. 2023. Vol. 231. N 107276. DOI: 10.1016/j.catena.2023.107276

5. Shuguang Lu, Li Wu, Chunmei Ma et al. Shifting sediment sources track environmental changes since the last glacial period: Evidence from sediment records in Chaohu Lake, eastern China. *Quaternary Science Reviews*. 2025. Vol. 365. N 109472. DOI: 10.1016/j.quascirev.2025.109472

6. Maslennikova A.V., Udachin V.N., Deryagin V.V. Paleoecology and geochemistry of the lake sedimentation of the Urals. Ekaterinburg: RIO UrO RAN, 2014, p. 136 (in Russian).

7. Nigamatzyanova G.R., Frolova L.A., Nigmatullin N.M. et al. Vegetation and climate changes in the Southern Urals in the Late Glacial and Holocene derived from pollen record of Lake Bolshoe Miassovo. *Geomorfologiya i paleogeografiya.* 2023. Vol. 54. N 4, p. 179-194 (in Russian). DOI: 10.31857/S2949178923040060

8. Valieva E.A., Frolova L.A., Palagushkina O.V. et al. Late Glacial and Holocene history of Lake Bolshoe Miassovo (Southern Urals) based on diatom analysis of bottom sediments. *Geomorfologiya i paleogeografiya.* 2023. Vol. 54. N 4, p. 195-206 (in Russian). DOI: 10.31857/S2949178923040151

9. Yusupova A.R., Kuzina D.M., Kosareva L.R. et al. Geochemistry and mineralogy of sediments of lakes in the Southern Urals. Mineraly: stroenie, svoistva, metody issledovaniya: Materialy X Vserossiiskoi molodezhnoi nauchnoi konferentsii, 27-31 May 2019, Ekaterinburg, Rossiya. Ekaterinburg: Institut geologii i geokhimii Uralskogo otdeleniya RAN, 2019. 2019, p. 292-293 (in Russian).

10. Sigov A.P., Shub V.S. Geomorphological regionalization of the Urals. Materialy po geomorfologii i noveishei tektonike Urala i Povolzhya. Ufa: Akademiya nauk SSSR, Bashkirskii filial, Institut geologii, 1972. N 3, p. 44-51 (in Russian).

11. State Geological Map of the Russian Federation. Scale 1:200,000. 2nd ed. Southern Ural series. Sheet N-41-VII. Explanatory note. Moscow: Moskovskii filial VSEGEI, 2015 (in Russian).

12. Bronk Ramsey C., Lee S. Recent and Planned Developments of the Program OxCal. *Radiocarbon*. 2013. Vol. 55. Iss. 2: Proceedings of the 21st International Radiocarbon Conference (Part 1 of 2), p. 720-730. DOI: 10.1017/S0033822200057878

13. Kuzina D.M., Shcherbakov V.P., Salnaia N.V. et al. Relative Paleointensity of Geomagnetic Field over the Past 9000 Years Estimated by the Pseudo-Thellier Method from the Bottom Sediments of Lake Shira, Northern Khakassia. *Izvestiya, Physics of the Solid Earth.* 2024. Vol. 60. N 4, p. 663-680. DOI: 10.1134/S1069351324700587

14. Cox R., Lowe D.R., Cullers R.L. The influence of sediment recycling and basement composition on evolution of mudrock chemistry in the southwestern United States. *Geochimica et Cosmochimica Acta*. 1995. Vol. 59. Iss. 14, p. 2919-2940. DOI: 10.1016/0016-7037(95)00185-9

15. Nurgaliev D.K., Yasonov P.G. Utility model patent RU 81805: Coercivity spectrometer. Publ. 27.03.2009. Bull. N 7 (in Russian).

16. Kosareva L.R., Nourgaliev D.K., Kuzina D.M. et al. Ferromagnetic, dia-/paramagnetic and superparamagnetic components of Aral Sea sediments: significance for paleoenvironmental reconstruction. *ARPN Journal of Earth Sciences.* 2015. Vol. 4. N 1, p. 1-6.

17. Yusupova A.R., Nurgalieva N.G., Kuzina D.M. et al. Lithological features of Lake Bannoe sediments (Southern Urals) as an indicator of environmental and climate changes in the Holocene. *Lithosphere.* 2024. Vol. 24. N 1, p. 173-194 (in Russian). DOI: 10.24930/1681-9004-2024-24-1-173-194

18. Leusova N.Yu. Stability and preservation of biogenic forms of silica in coals. *Advances in current natural sciences.* 2020. N 12, p. 117-123 (in Russian). DOI: 10.17513/use.37547

19. Xiugen Fu, Jian Wang, Chunyan Song et al. The Permian-Triassic transition in ocean island setting: Environmental disturbances and new high-resolution carbon-isotope record from the Qiangtang Basin, NW China. *Palaeogeography, Palaeoclimatology, Palaeoecology*. 2019. Vol. 522, p. 40-51. DOI: 10.1016/j.palaeo.2019.03.012

20. Rudnick R.L., Gao S. Composition of the Continental Crust. Treatise on Geochemistry. Elsevier, 2003. Vol. 3, p. 1-64. DOI: 10.1016/B0-08-043751-6/03016-4

21. Yusupova A.R., Nurgalieva N.G., Kuzina D.M. et al. Composition characteristics of Sabakty Lake lacustrine sediments (Southern Urals). *Advances in current natural sciences.* 2023. N 7, p. 72-81 (in Russian). DOI: 10.17513/use.38074

22. Yusupova A.R., Nourgalieva N.G., Kuzina D.M., H.-Ch. Li. The Composition of Lacustrine Sediments of Lake Kandrykul (Republic of Bashkortostan) Based on Mineralogical, Geochemical Data and Climatic Changes in the Holocene. *Georesursy.* 2025. Vol. 27. N 2, p. 281-296 (in Russian). DOI: 10.18599/grs.2025.2.21

23. Ecology of Lake Bolshoye Miassovo. Ed. by A.G.Rogozin, V.A.Tkachev. Miass: Ilmenskii gosudarstvennyi zapovednik im. V.I.Lenina UrO RAN, 2000, p. 318 (in Russian).

24. Snachev V.I., Snachev A.V., Rykus M.V. Physical and chemical conditions of generation and formation belonging to Kisegachsky granitoid massiv (South Ural). *Petroleum Engineering.* 2020. Vol. 18. N 5, p. 6-14 (in Russian). DOI: 10.17122/ngdelo-2020-5-6-14

25. Kalugin I., Daryin A., Smolyaninova L. et al. 800-yr-long records of annual air temperature and precipitation over southern Siberia inferred from Teletskoye Lake sediments. *Quaternary Research*. 2007. Vol. 67. Iss. 3, p. 400-410. DOI: 10.1016/j.yqres.2007.01.007

26. Korinevsky V.G., Korinevsky E.V. Results of geological-petrographic study of 1998-2018 of the Ilmenogorsky complex, South Urals. *Mineralogy.* 2020. Vol. 6. Iss. 2, p. 67-99 (in Russian). DOI: 10.35597/2313-545X-2020-6-2-6

27. Smith J.V., Brown W.L. Feldspar Minerals. Vol. 1. Crystal Structures, Physical, Chemical, and Microtextural Properties. Springer-Verlag, 1988, p. 846. DOI: 10.1007/978-3-642-72594-4

28. Popov N., Marijan S., Pavić L. et al. Influence of $Al^{3+}$ ions on the direct hydrothermal formation and properties of hematite (α-$Fe_2O_3$) nanorods. *Journal of Alloys and Compounds*. 2025. Vol. 1018. N 179223. DOI: 10.1016/j.jallcom.2025.179223

29. Cherniak D.J. Aluminum diffusion in zircon. *Chemical Geology*. 2021. Vol. 584. N 120510. DOI: 10.1016/j.chemgeo.2021.120510

30. Lange I.M., Reynolds R.C., Lyons J.B. KRb ratios in coexisting K-feldspars and biotites from some New England granites and metasediments. *Chemical Geology*. 1966. Vol. 1, p. 317-322. DOI: 10.1016/0009-2541(66)90027-1

31. Igneous Rocks: A classification and glossary of terms. Recommendations of the International Union of Geological Sciences Subcommission on the Systematics of Igneous Rocks. Ed. by R.W. Le Maitre. Cambridge University Press, 2002, p. 252. DOI: 10.1017/CBO9780511535581

32. Rhodes J.M. On the chemistry of potassium feldspars in granitic rocks. *Chemical Geology*. 1969. Vol. 4. Iss. 3-4, p. 373-392. DOI: 10.1016/0009-2541(69)90004-7

33. Usui H., Domi Y., Sakaguchi H. Rutile TiO2 Creates Advanced Na-Storage Materials. *ACS Applied Energy Materials*. 2023. Vol. 6. Iss. 8, p. 4089-4102. DOI: 10.1021/acsaem.3c00266

34. Rashchenko S., Shatskiy A., Litasov K. High-Pressure Na-Ca Carbonates in the Deep Carbon Cycle. *Carbon in Earth's Interior*. Wiley, 2020, p. 127-136. DOI: 10.1002/9781119508229.ch13

35. Bernard E., Yio M., Rentsch D. et al. Insights on the effects of carbonates and phosphates on the hydration of magnesia (alumino-)silicate cements. *Applied Geochemistry*. 2024. Vol. 167. N 106001. DOI: 10.1016/j.apgeochem.2024.106001

36. Baijot M., Hatert F., Philippo S. Mineralogy and geochemistry of phosphates and silicates in the Sapucaia pegmatite, Minas Gerais, Brazil: genetic implications. *The Canadian Mineralogist*. 2012. Vol. 50. N 6, p. 1531-1554. DOI: 10.3749/canmin.50.6.1531

37. Zaccarini F., Garuti G., Moser R. et al. Mineral Chemistry of Olivine, Oxy-Spinel, and Clinopyroxene in Lavas and Xenoliths from the Canary, Azores, and Cape Verde Islands (Macaronesia, North Atlantic Ocean): New Data and Comparisons with the Literature. *Minerals*. 2024. Vol. 14. Iss. 2. N 161. DOI: 10.3390/min14020161

38. Hermann J., O'Neill H.S.C., Berry A.J. Titanium solubility in olivine in the system $TiO_2$-MgO-$SiO_2$: no evidence for an ultra-deep origin of Ti-bearing olivine. *Contributions to Mineralogy and Petrology*. 2005. Vol. 148. Iss. 6, p. 746-760. DOI: 10.1007/s00410-004-0637-4

39. Santisteban J.I., Mediavilla R., López-Pamo E. et al. Loss on ignition: a qualitative or quantitative method for organic matter and carbonate mineral content in sediments? *Journal of Paleolimnology*. 2004. Vol. 32. Iss. 3, p. 287-299. DOI: 10.1023/B:JOPL.0000042999.30131.5b

40. Yudovich Ya.E., Ketris M.P. Geochemical Indicators of Lithogenesis. Syktyvkar: Geoprint, 2011, p. 742 (in Russian).

41. Yudovich Ya.E., Ketris M.P. Mineral Indicators of Lithogenesis. Syktyvkar: Geoprint, 2008, p. 564 (in Russian).

42. Qing Sun, Daryin A., Jiayu Zhao et al. High-Resolution Elemental Record from the Holocene Sediments of an Alpine Lake in the Central Altai Mountains: Implications for Arctic Sea-Ice Variations. *Earth and Space Science*. 2021. Vol. 8. Iss. 8. N e2021EA001810. DOI: 10.1029/2021EA001810

43. Ziwei Long, Zehua Ji, Yuansheng Pei. Characteristics and distribution of phosphorus in surface sediments of a shallow lake. *Journal of Environmental Sciences*. 2023. Vol. 124, p. 50-60. DOI: 10.1016/j.jes.2021.10.012

44. DoĞan M., Ünlü Y., Gürboğa Ş. et al. Climate variability in West Anatolia from Last Glacial Maximum to present based on the µXRF data from Buldan Yayla Lake (Denizli). *Journal of Quaternary Science*. 2025. Vol. 40. Iss. 1, p. 86-105. DOI: 10.1002/jqs.3658

45. López-Sáez J.A., Carrasco R.M., Turu V. et al. Late Glacial-early holocene vegetation and environmental changes in the western Iberian Central System inferred from a key site: The Navamuño record, Béjar range (Spain). *Quaternary Science Reviews*. 2020. Vol. 230. N 106167. DOI: 10.1016/j.quascirev.2020.106167

46. Maslennikova A.V., Artemiev D.A., Zazovskaia E.P. et al. Geochemical record of Lake Sabakty: Electrical conductivity and reconstruction of the Lateglacial and Holocene environments in the Southern Urals (Russia) steppe. *Lithosphere*. 2023. Vol. 23. N 3, p. 410-429 (in Russian). DOI: 10.24930/1681-9004-2023-23-3-410-429

47. Qimei Guo, Baohua Li, Yue Cai. Intermediate water circulation in the mid-latitude Northeast Atlantic over the past 13,000 years: Multi-proxy evidence from IODP Site U1391. *Palaeogeography, Palaeoclimatology, Palaeoecology*. 2024. Vol. 654. N 112428. DOI: 10.1016/j.palaeo.2024.112428

48. Walker M., Head M.J., Berkelhammer M. et al. Formal ratification of the subdivision of the Holocene Series/Epoch (Quaternary System/Period): two new Global Boundary Stratotype Sections and Points (GSSPs) and three new stages/subseries. *Episodes*. 2018. Vol. 41. N 4, p. 213-223. DOI: 10.18814/epiiugs/2018/018016

49. Walker M.J.C., Berkelhammer M., Björck S. et al. Formal subdivision of the Holocene Series/Epoch: a Discussion Paper by a Working Group of INTIMATE (Integration of ice-core, marine and terrestrial records) and the Subcommission on Quaternary Stratigraphy (International Commission on Stratigraphy). *Journal of Quaternary Science*. 2012. Vol. 27. Iss. 7, p. 649-659. DOI: 10.1002/jqs.2565

***Authors*: Anastasiya R. Yusupova,** *Candidate of Geological and Mineralogical Sciences, Senior Researcher (Kazan Federal University, Kazan, Republic of Tatarstan, Russia), i@ajusupova.ru, https://orcid.org/0000-0001-8732-3053*, **Nouria G. Nourgalieva,** *Doctor of Geological and Mineralogical Sciences, Professor (Kazan Federal University, Kazan, Republic of Tatarstan, Russia), https://orcid.org/0000-0003-4372-9777*.

*The authors declare no conflicts of interests.*